Nonlinear beat wave decay of Kelvin/diocotron waves on a two-dimensional vortex

Cite as: Phys. Fluids **36**, 034121 (2024); doi: 10.1063/5.0190218
Submitted: 4 December 2023 · Accepted: 25 February 2024 ·
Published Online: 19 March 2024

Daniel H. E. Dubin,[a] A. A. Kabantsev, and C. F. Driscoll

AFFILIATIONS

Department of Physics UCSD, La Jolla, California 92093, USA

Note: This paper is part of the special topic, Coherent Vortical Structures in Fluids and Plasmas.
[a]**Author to whom correspondence should be addressed:** ddubin@ucsd.edu

ABSTRACT

We describe theory and experiments investigating nonlinear beat wave decay of diocotron modes on a nonneutral plasma column (or Kelvin waves on a vortex). Specifically, a Kelvin/diocotron pump wave varying as $A_p \exp[i(l_p\theta - \omega_p t)]$ decays into two waves: a Kelvin/diocotron daughter wave with exponentially growing amplitude $A_d(t)$, mode number $l_d < l_p$, and frequency ω_d; and an exponentially growing "beat wave" with mode number l_b and frequency ω_b. Nonlinear wave–wave coupling requires $l_b = l_p - l_d$ and $\omega_b = \omega_p - \omega_d$. The new theory simplifies and extends a previous weak-turbulence theory for the exponential growth rate of this instability, by instead using an eigenmode expansion to describe the beat wave as a wavepacket of continuum (Case/van Kampen) modes. The new theory predicts the growth rate, the nonlinear frequency shift (both proportional to A_p^2), and the functional form of the beat wave, with amplitude proportional to $A_p A_d^*(t)$. Experiments observe beat wave decay on electron plasma columns for a range of mode numbers up to $l_p = 5$ and $l_d = 4$, with results in quantitative agreement with the theory, including the $l_d = 1$ case for which measured growth rates are negligible, as expected theoretically.

I. INTRODUCTION

The phenomenon of self-organization, in which fluctuation energy in a fluid flow is transferred from smaller to larger spatial scales, plays an important role in a range of physical processes in both fluids and plasmas. Examples include the generation of zonal flows,[1] the merger of like-sign vortices,[2] and the formation of vortex crystals[3] and other coherent structures[4] from turbulent states.

Another manifestation of self-organization is the spontaneous symmetrization of a single isolated vortex,[5–10] in which asymmetries initially present on the vortex decay through inviscid processes. One such process, spatial Landau damping of the asymmetry, is associated with a critical layer that occurs at a resonance between the rotation rate of the vortex and the phase velocity of the asymmetry (a "direct" resonance).[11,12] However, this direct resonance process does not occur for vortices with edges that are sufficiently sharp so that the resonance condition is satisfied at a radius outside the vortex. Nevertheless, axisymmetrization can still occur through a different inviscid process, in which nonlinear couplings between asymmetries present in the vortex transfer energy from larger wavenumber asymmetries to smaller wavenumbers (sometimes referred to as down-scattering[13]) We will see that this nonlinear axisymmetrization process is also driven by a resonance at a critical layer, but the resonance is at a different radial location, within the vortex. Theoretical and experimental investigations of this nonlinear axisymmetrization process are this subject of this paper.

Previous experiments[13–15] have observed this nonlinear axisymmetrization in a pure electron plasma, which closely mimics the dynamics of an ideal inviscid 2D fluid[16] (i.e., a 2D Euler flow). In these experiments, a nominally cylindrically symmetric vortex is perturbed in a controlled fashion to induce a Kelvin "pump" wave on the surface of the vortex (termed a diocotron mode in the plasma literature). The pump wave is a traveling wave that has time and θ dependence of the form $\cos(l_p\theta - \omega_p t + \psi_p)$, where ψ_p is an arbitrary phase, $l_p > 1$ is the azimuthal mode number of the pump wave and $\omega_p > 0$ is the pump wave frequency. This wave is observed to decay in amplitude through the excitation and exponential growth of a second Kelvin/diocotron "daughter" wave with mode number l_d, $0 < l_d < l_p$, and with frequency ω_d, $0 < \omega_d < \omega_p$. (The terms pump wave and daughter wave are taken from the theory of parametric oscillators.) This process is mediated by a third wave, termed a beat wave, with mode number $l_b = l_p - l_d$, which is driven at the beat frequency $\omega_b = \omega_p - \omega_d$ by the nonlinear coupling of the two Kelvin/diocotron waves, and which couples back to these waves to induce the growth of the daughter wave. Thus, this process is similar in some respects to a standard three-wave decay instability.[17] However, the beat wave is not a Kelvin/

diocotron wave with mode number l_b. The beat wave is instead, primarily, a wavepacket of the continuum eigenmodes[18] of the vortex. Its phase velocity ω_b/l_b is resonant with the vortex rotation at a critical layer within the vortex, and the resulting strong spatial Landau damping induced by this resonance is what drives the decay of the pump wave, along with growth of the daughter wave. We, therefore, refer to this decay process as a beat wave decay instability, to distinguish it from three-wave decay.

A previous publication[13] described this beat wave decay process using a theoretical approach based on a weak turbulence expansion of the nonlinear equations of motion to third order in perturbed quantities (i.e., one higher order than that required for a description of three-wave processes). This weak turbulence approach has several antecedents in the plasma and astrophysics literature, having been applied to analyze various nonlinear wave interactions,[19–21] including instabilities similar to the beat wave decay process considered here.[22,23]

In this paper, we describe beat wave decay from a different perspective, based on an eigenmode expansion of the system dynamics. These eigenmodes, consisting of the Kelvin/diocotron modes and continuum modes, form a complete orthogonal set, with orthogonality defined by an inner product based either on energy or on angular momentum conservation. We work in the rotating frame of the pump wave, in which the wave is, in the initial phase of the instability, a stationary equilibrium state. The beat wave instability is then described as a single unstable eigenmode of the perturbed pump wave equilibrium, whose frequency and growth rate can be analyzed (for small pump amplitudes) using perturbation theory of the system eigenfrequencies. In the perturbation theory, we represent this unstable eigenmode as a wavepacket of the eigenmodes (Kelvin/diocotron and continuum) of the unperturbed vortex. This eigenmode approach to analyzing nonlinear instability also has many antecedents.[24–27] The eigenmode approach allows a detailed and physically intuitive analysis of the beat wave process, in which explicit expressions are obtained for the instability growth rate, the real frequency shift, and the beat wave vorticity and stream function perturbations. We compare these predictions to new experiments that observe the beat wave decay for a range of decay processes, for pump waves up to mode number $l = 5$ and every possible daughter wave mode number.

The paper is laid out as follows: Sec. II contains a review of known theoretical results that will be of use in describing beat wave decay, including brief discussions of the connection between nonneutral plasma dynamics and the Euler equations, constants of the motion, the linear eigenmodes of the Euler equations including the Kelvin waves (diocotron modes) and continuum eigenmodes, and inner product relations for these modes. We also include here some new results regarding the evaluation of the continuum modes. Section III analyzes the beat wave decay process, including a detailed description of the beat wave instability as well as nonlinear frequency shifts to both the pump and daughter waves. Section IV discusses the results of new nonneutral plasma experiments that observe beat wave decay, with comparisons to the theory. Section V summarizes the results. Finally, the Appendix contains some derivations of intermediate results, including a proof of the equivalence of two expressions for the beat wave instability growth rate.

II. PRELIMINARIES

In this section, we review some well-known results and also derive some new results, concerning the linear evolution of perturbations on an isolated vortex. These results will then be applied, in Sec. III, to the evolution of the nonlinear beat wave decay instability.

A. 2D equations of motion for ideal fluids and magnetized plasmas

The Euler equations for the evolution of vorticity $n(r,\theta,t)$ in a 2D ideal (dissipationless) incompressible fluid with uniform mass density ρ_0 per unit area are

$$\frac{\partial n}{\partial t} + \mathbf{v}\cdot\nabla n = 0, \tag{1}$$

where the fluid velocity $\mathbf{v}(r,\theta,t)$ is related to the stream function ϕ through

$$\mathbf{v} = \nabla\phi\times\hat{z} = \hat{r}\,\frac{1}{r}\frac{\partial\phi}{\partial\theta} - \hat{\theta}\,\frac{\partial\phi}{\partial r}, \tag{2}$$

and the stream function $\phi(r,\theta,t)$ is determined in terms of the vorticity n by $n = \hat{z}\cdot\nabla\times\boldsymbol{v}$, which after using Eq. (2), yields

$$\nabla^2\phi = -n. \tag{3}$$

In this paper, we use a free-slip boundary condition $\phi = 0$ on a surrounding cylindrical wall at radius $r = r_w$, so there is no dissipative coupling to the wall.

Applying Eq. (2) to Eq. (1) yields another form for the vorticity continuity equation,

$$\frac{\partial n}{\partial t} + \frac{1}{r}\frac{\partial\phi}{\partial\theta}\frac{\partial n}{\partial r} - \frac{1}{r}\frac{\partial\phi}{\partial r}\frac{\partial n}{\partial\theta} = 0. \tag{4}$$

It is well known that these equations are isomorphic to the equations of motion for 2D $E\times B$ drift dynamics of a collisionless nonneutral plasma column contained in hollow cylindrical electrodes, with plasma length much greater than the electrode inner radius r_w, in a uniform magnetic field $-B\hat{z}$, $B>0$. The plasma consists of like charges $e>0$ with z-averaged number density $N(r,\theta,t)$, creating an electrostatic potential $\Phi(r,\theta,t)$. The stream function ϕ is then proportional to the potential Φ, $\phi = c\Phi/B$; the vorticity n is related to plasma density N through $n = 4\pi ecN/B$; and the fluid velocity $\boldsymbol{v}$ is the same in both plasma and fluid systems. The boundary condition $\phi(r_w) = \Phi(r_w) = 0$ corresponds to a grounded electrode. [Note: for a pure electron plasma consisting of like charges $-e$, sign changes in two of the above relations are necessary: the magnetic field is now in the $+z$ direction, $+B\hat{z}$ with $B>0$, and $\phi = -c\Phi/B$. Using these sign conventions all other equations in the paper are independent of the sign of plasma charge, unless directly specified.]

It is useful to Fourier transform in θ, writing n and ϕ as

$$n = \sum_{l=-\infty}^{\infty} n_l(r,t)e^{il\theta}, \tag{5}$$

$$\phi = \sum_{l=-\infty}^{\infty} \phi_l(r,t)e^{il\theta}. \tag{6}$$

Mode numbers less than zero satisfy $n_{-l} = n_l^*$, $\phi_{-l} = \phi_l^*$ in order for the sums to yield real quantities.

Then, when written in terms of Fourier modes Eq. (4) becomes

$$\frac{\partial n_l}{\partial t} + \frac{i}{r}\sum_{\bar{l}=-\infty}^{\infty}\bar{l}\left(\phi_{\bar{l}}\frac{\partial n_{l-\bar{l}}}{\partial r} - n_{\bar{l}}\frac{\partial\phi_{l-\bar{l}}}{\partial r}\right) = 0, \tag{7}$$

and the Poisson Eq. (3) is

$$\frac{\partial^2\phi_l}{\partial r^2}+\frac{1}{r}\frac{\partial\phi_l}{\partial r}-\frac{l^2}{r^2}\phi_l=-n_l. \tag{8}$$

B. Constants of motion

We will later have occasion to consider constants of the motion. In the ideal fluid system, there are an infinite number of constants of the motion, but here we will consider three: energy, angular momentum, and particle number (equivalent to circulation).

In an ideal 2D Euler fluid with free-slip boundary conditions described previously, the circulation $\Gamma=\int d^2rn$ is a conserved quantity. In the plasma analog, the corresponding conserved quantity is the particle number per unit length $\int d^2rN$.

In the fluid system, total kinetic energy is another conserved quantity, given by $\mathscr{K}=\frac{\rho_0}{2}\int d^2r|\boldsymbol{v}|^2=\frac{\rho_0}{2}\int d^2r|\nabla\phi|^2$. In the plasma case, the analogous conserved energy in 2D drift dynamics is $\mathscr{E}=\frac{1}{8\pi}\int d^2r|\nabla\Phi|^2$, the potential energy per unit length in the plasma column. The fluid and plasma energies are then related according to

$$\mathscr{E}=\frac{B^2}{4\pi\rho_0c^2}\mathscr{K}. \tag{9}$$

In addition, the cylindrical free-slip boundary condition implies that total angular momentum of the fluid, $\mathscr{P}=\rho_0\int d^2rrv_\theta$, is a conserved quantity. Using Eq. (2) for v_θ and integrating by parts, the angular momentum can be written in terms of integrals over the vorticity,

$$\mathscr{P}=\frac{1}{2}\rho_0r_w^2\Gamma-\frac{\rho_0}{2}\int d^2rr^2n. \tag{10}$$

In the plasma case, the quantity analogous to the second term in this expression is the canonical angular momentum for charges in a uniform magnetic field, $\mathscr{P}_\theta=-\frac{eB}{2c}\int d^2rNr^2$. The relation between the fluid and plasma angular momenta is

$$\mathscr{P}_\theta=\frac{B^2}{4\pi\rho_0c^2}\left(\mathscr{P}-\frac{1}{2}\rho_0r_w^2\Gamma\right). \tag{11}$$

C. Kelvin waves/diocotron modes

In this subsection, we briefly review some properties of linear oscillations associated with the two dimensional incompressible fluid dynamics described by Eqs. (7) and (8). Assume that the $l=0$ Fourier component of the vorticity describes a cylindrically symmetric equilibrium vortex of vorticity $n_e(r)$ and stream function $\phi_e(r)$. Then, small amplitude excitations about that equilibrium, with azimuthal mode number l, may be described by the linearized version of Eq. (7),

$$\frac{\partial n_l}{\partial t}+il\omega_e(r)n_l+\frac{il}{r}\frac{\partial n_e}{\partial r}\phi_l=0, \tag{12}$$

where $\omega_e(r)=-\phi_e'(r)/r$ is the sheared rotation frequency of the equilibrium vortex. (Here and throughout the paper primes refer to radial derivatives.) Since the coefficient functions in Eq. (12) are time-independent, solutions for n_l that are proportional to $\exp(-i\omega t)$ can be found. These oscillating solutions are linear eigenmodes of the system. The oscillatory time-dependence implies that Eq. (12) can be written as

$$\omega n_l=l\omega_en_l+\frac{l}{r}\frac{\partial n_e}{\partial r}\phi_l \tag{13}$$

Equation (13) can be solved for n_l in terms of ϕ_l and the result applied to Eq. (8), to yield the following differential equation for the lth Fourier component of the stream function, ϕ_l,

$$\frac{\partial^2\phi_l}{\partial r^2}+\frac{1}{r}\frac{\partial\phi_l}{\partial r}-\frac{l^2}{r^2}\phi_l+\frac{l}{r(\omega-l\omega_e)}\frac{\partial n_e}{\partial r}\phi_l=0, \tag{14}$$

with boundary condition that $\phi_l(r_w)=0$. By correct choice of ω, nontrivial solutions $\phi_l(r)=\phi_{l,K}(r)$ can sometimes be found. These nontrivial solutions are called Kelvin waves in the fluid literature and diocotron waves in the plasma literature. For an equilibrium vorticity profile $n_e(r)$ that is monotonically decreasing [so that $\omega_e(r)$ is also monotonically decreasing] there may be a Kelvin/diocotron mode solution $\phi_{l,K}(r)$ of Eq. (14) with real frequency $\omega_{l,K}$. However, this solution can only be found if the resonant radius $r_{l,K}$ that satisfies $\omega_{l,K}=l\omega_e(r_{l,K})$ is at a location with no vorticity gradient, so that the denominator in Eq. (14) is only zero for a radius $r_{l,K}$ at which $n_e'(r_{l,K})=0$.

Note that for any eigenmode with $l>0$, there is a corresponding eigenmode with $l<0$, with frequency $\omega_{-l,K}=-\omega_{l,K}$, and stream function $\phi_{-l,K}=\phi_{l,K}^*$. The negative l eigenmodes are merely complex conjugates of the $l>0$ eigenmodes, but are still required for completeness, in order to form real functions out of sums of eigenmodes.

These Kelvin/diocotron eigenmodes are $l\neq0$ traveling waves in the θ direction on the surface of the vortex, with positive phase velocity $\omega_{l,K}/l$. For a vortex of uniform vorticity n_e with radius r_p, the Kelvin/diocotron frequency is[28]

$$\omega_{l,K}=\mathrm{sign}(l)\omega_e\left[|l|-1+\left(\frac{r_p}{r_w}\right)^{|2l|}\right], \tag{15}$$

where $\omega_e=n_e/2$ is the rotation frequency of the equilibrium vortex. Each mode (summed to its complex conjugate mode) corresponds to time-dependent variation in the shape $R(\theta,t)$ of the vortex of the form

$$R(\theta,t)/r_p-1=a_l(t)\exp(il\theta)+\text{c.c.}, \tag{16}$$

where

$$a_l(t)=A_l\exp(-i\omega_{l,K}t) \tag{17}$$

is the dimensionless perturbation to the vortex radius and A_l is the dimensionless complex amplitude of this perturbation.

For $l=1$, the Kelvin/diocotron solution can be found analytically for general vorticity profiles,

$$\begin{aligned}\omega_{1,K}&=\omega_e(r_w)=\frac{\Gamma}{2\pi r_w^2},\\ \phi_{1,K}(r)&=-Ar(\omega_{1,K}-\omega_e(r)),\\ n_{1,K}(r)&=-An_e'(r),\end{aligned} \tag{18}$$

where A is an arbitrary amplitude equal to A_1r_p for the case of a uniform vortex patch. This mode is a displacement of the center of the vortex, which then rotates about the axis of the cylinder at the mode frequency $\omega_{1,K}$ due to its interaction with "image vortices" in the cylindrical wall.

For higher mode numbers l and for general radial vorticity profiles, Eq. (14) can be solved numerically, for example, using a shooting method, to determine the perturbed stream function ϕ_l and vorticity n_l of a Kelvin/diocotron wave. For future reference, we define a dimensionless radial perturbation amplitude a_l in terms of the lth multipole moment of the vorticity,

$$a_l(t) = \frac{\int d^2r\, n(r,\theta,t) r^l e^{-il\theta}}{(l+2)\int d^2r\, n(r,\theta,t) r^l} = \frac{\int rdr\, n_l(r,t) r^l}{(l+2)\int rdr\, n_e(r) r^l}, \tag{19}$$

which agrees with Eq. (16) for a Kelvin/diocotron mode on a uniform vortex of radius r_p.

Examples of the Kelvin/diocotron stream functions $\phi_{l,K}$ for the first five modes are shown in Fig. 1 for an equilibrium vorticity profile $n_e(r)$ shown in Fig. 2. This profile is close to one generated in nonneutral plasma experiments with a wall radius $r_w = 3.5$ cm, discussed in Sec. IV.

In the figure, Kelvin/diocotron eigenmodes are all scaled in amplitude so that their corresponding dimensionless amplitudes A_l equal unity. We use this normalization for Kelvin/diocotron eigenmodes throughout the paper.

D. Continuum modes

There is a second approach to finding the eigenmodes of an isolated vortex, which identifies a complete set of eigenmodes, including a set of continuum modes. The continuum modes in sheared Euler flow were first identified by Case[18] and are analogous, and play a similar role, to the van Kampen continuum in plasma kinetic theory.[29] We will briefly review the properties of these Case/van Kampen continuum modes and also discuss some new results that will be useful later in the description of the nonlinear beat wave instability.

Equation (13) for the linear eigenmodes of the perturbed vortex equilibrium can be written as an integral equation involving the Green's function for the stream function ϕ_l,

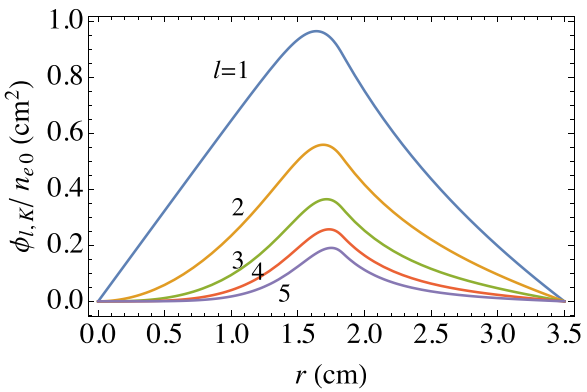

FIG. 1. Kelvin/diocotron mode stream functions $\phi_{l,K}$ for azimuthal mode numbers $l = 1, \ldots, 5$, each scaled to n_{e0} where $n_{e0} = n_e(r = 0)$ is the central vorticity, for the equilibrium vorticity profile shown in Fig. 2. These eigenmodes have amplitudes chosen so that their dimensionless amplitudes A_l equal unity. This normalization is used for Kelvin/diocotron eigenmodes throughout the paper.

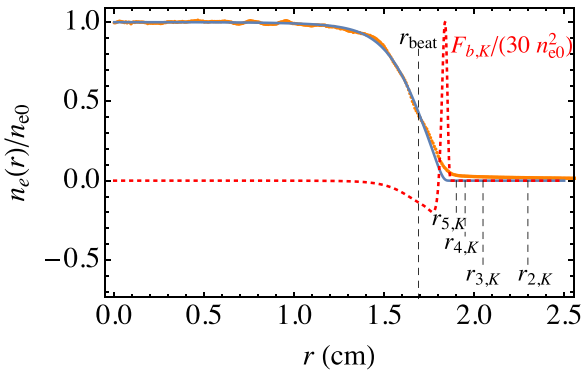

FIG. 2. Equilibrium vorticity profile $n_e(r)$ used throughout the paper (smooth solid black curve), and the locations of the resonant radii $r_{2,K}, r_{3,K}, r_{4,K}, r_{5,K}$, as well as the beat wave resonant radius r_{beat} for $3 \rightarrow 2$ decay. The noisy data (red curve) is the equilibrium density profile measured in the experiment. Also shown is the beat wave forcing function $F_{b,K}(r)$ for $3 \rightarrow 2$ decay (dotted line); see Eq. (54).

$$\omega n_l = l\omega_e n_l + \frac{l}{r}\frac{\partial n_e}{\partial r}\hat{G}_l n_l \equiv \hat{L}_l n_l, \tag{20}$$

where $\hat{G}_l$ is the Greens function operator,

$$\phi_l = \hat{G}_l n_l = -\int r'dr' G_l(r,r') n_l(r') \tag{21}$$

with

$$G_l(r,r') = -\frac{1}{|2l|}\left(\frac{r_<}{r_>}\right)^{|l|}\left[1 - \left(\frac{r_>}{r_w}\right)^{|2l|}\right]. \tag{22}$$

Equation (20) is an eigenvalue problem for the operator $\hat{L}_l$, determining an infinite set of vorticity eigenfunctions $n_{l,\alpha}(r)$ with corresponding real frequencies $\omega_{l,\alpha}$ in the range $\omega_e(0) \geq \omega_{l,\alpha}/l > \omega_e(r_w)$, where α is a counter that enumerates the eigenmodes. One of these eigenmodes is the vorticity perturbation corresponding to the Kelvin/diocotron mode found using the previous method, Eq. (14), if such a mode exists. The other eigenmodes are continuum modes with singular radial dependence, i.e., a Dirac delta function in the vorticity perturbation at radius $r_{l,\alpha}$ given by the solution to the resonance equation,

$$\omega_{l,\alpha} = l\omega_e(r_{l,\alpha}). \tag{23}$$

These singular continuum eigenfunctions do not appear in the previous solution of Eq. (14), because there we divided by $\omega - l\omega_e(r)$ assuming that it is nonzero everywhere that $n_e'(r)$ is nonzero.

The continuum modes can be determined numerically, for example, by discretizing the radial dimension, converting Eq. (20) into a standard matrix eigenvalue problem.[11] An example of the resulting discretized frequency spectrum is shown in Fig. 3 for $l = 2$ using the equilibrium vorticity profile of Fig. 2, setting $n_e'(r) = 0$ for all radii r greater than some radius R chosen to be smaller than the resonant radius $r_{l,K}$ of the Kelvin/diocotron mode, which equals 2.3 cm for this vorticity profile (see Fig. 2). We, therefore, choose $R = 2.1$ cm. Figure 3 shows that the continuum modes form a band of frequencies satisfying Eq. (23) for resonant radii in the range $0 < r_{l,\alpha} \leq R$, while the Kelvin/diocotron mode frequency falls outside this band, and for this reason is sometimes referred to as a "discrete eigenmode."

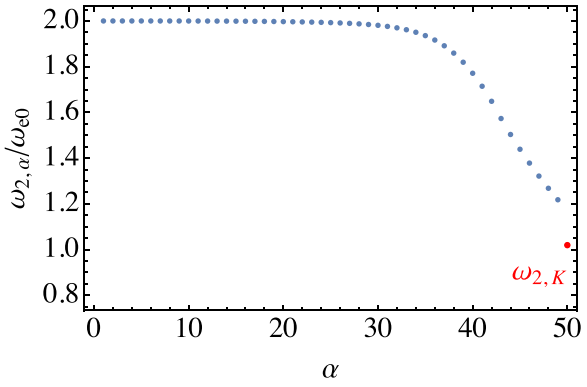

FIG. 3. Frequency spectrum of eigenmodes found by discretizing the radial dimension in Eq. (20) for $l=2$, taking $r=i\Delta r, i=1,\ldots,M$, for $\Delta r=R/M, M=50$, and $R=2.1$ cm. Frequencies are scaled to $\omega_{e0}=n_{e0}/2$, the vortex rotation frequency at $r=0$.

If we had instead chosen $R>r_{l,K}$ in Fig. 3, the discrete mode would then be manifested as a wavepacket of continuum modes. If one excites the plasma using an external applied potential with mode number l and a broad frequency bandwidth, the resulting motion of the plasma may be dominated by this wavepacket, which is more or less sharply peaked in frequency around the original Kelvin/diocotron frequency $\omega_{l,K}$ depending on the magnitude of $n_e'(r_{l,K})$. When this resonant vorticity gradient is small, the wavepacket has a radial dependence close to that of the discrete Kelvin/diocotron mode found when $R<r_{l,K}$. The finite frequency width of this wavepacket induces phase-mixing in the time dependence of the packet, causing exponential "spatial Landau-damping" of the perturbation. The exponential damping rate can be predicted via a contour-deformation analysis of the solution to Eq. (14), assuming a complex frequency ω and deforming the radial integration path into a Landau contour around the pole.[11,12] Because the resulting damped mode is not a single eigenmode—it is a wavepacket of continuum eigenmodes—it is often referred to as a "quasimode." All of this has been covered in the referenced publications.

We now consider some new results involving the continuum eigenmodes that will be of use in the analysis of beat-wave decay. Numerical accuracy of the matrix method used to determine the continuum modes in Fig. 3 is limited by the difficulty of resolving a Dirac delta function using a discrete radial grid. There is a novel, more accurate approach. Using Eq. (13), it can be seen that the functional forms of the singular vorticity and stream function perturbations in a continuum eigenmode, $n_{l,\alpha}(r)$ and $\phi_{l,\alpha}(r)$, respectively, are related according to

$$n_{l,\alpha}=b\delta(r-r_{l,\alpha})+\frac{l}{r}n_e'(r)\phi_{l,\alpha}\frac{P}{\omega_{l,\alpha}-l\omega_e(r)}, \tag{24}$$

where b is an arbitrary normalization with units of velocity, and P denotes the principal part of the resonant denominator. The functions $n_{l,\alpha}$ and $\phi_{l,\alpha}$ are further related by the Poisson equation (8) yielding the ODE,

$$\frac{1}{r}\frac{\partial}{\partial r}\left(r\frac{\partial\phi_{l,\alpha}}{\partial r}\right)-\frac{l^2}{r^2}\phi_{l,\alpha}+\frac{l}{r}\frac{P}{\omega_{l,\alpha}-l\omega_e}\frac{\partial n_e}{\partial r}\phi_{l,\alpha}=-b\delta(r-r_{l,\alpha}), \tag{25}$$

with boundary condition $\phi_{l,\alpha}(r_w)=0$. Comparing this equation to Eq. (14), we can see that the continuum mode stream function $\phi_{l,\alpha}$ is akin to a Green's function for the regularized Kelvin/diocotron mode differential operator, with the source point $r_{l,\alpha}$ chosen to be the resonant radius satisfying Eq. (23). In this formulation, the stream function $\phi_{l,\alpha}$ solves a differential equation, allowing the application of high-accuracy numerical methods not available for integral equations such as Eq. (20).

In particular, one can employ such high-accuracy methods to numerically solve for two independent homogeneous solutions $\psi_a(r),\psi_b(r)$, with boundary conditions $\psi_a(0)=0=\psi_b(r_w)$. Standard analysis of the solutions near the regular singular point at $r=r_{l,\alpha}$ shows that these homogeneous solutions are finite and continuous there. The solutions are then connected across the delta function to obtain

$$\phi_{l,\alpha}(r)=-b\frac{\psi_a(r_<)\psi_b(r_>)}{W(r_{l,\alpha})}, \tag{26}$$

where the Wronskian $W(r)=\psi_a\psi_b'-\psi_b\psi_a'$ and where $r_{\gtrless}=\max_{\min}(r,r_{l,\alpha})$. Examples of the stream function of continuum modes are displayed in Fig. 4 for three values of the mode number l, taking the resonant radius to be $r_{l,\alpha}=1.5$ cm in each case.

Furthermore, for $l=1$ an analytic solution for the continuum modes is available,

$$\phi_{1,\alpha}(r)=\frac{br}{r_{1,\alpha}\omega_e'(r_{1,\alpha})}(\omega_e(r)-\omega_{1,\alpha})h(r_{1,\alpha}-r), \tag{27}$$

$$n_{1,\alpha}(r)=b\delta(r-r_{1,\alpha})-\frac{b}{r_{1,\alpha}\omega_e'(r_{1,\alpha})}n_e'(r)h(r_{1,\alpha}-r), \tag{28}$$

where $h(x)$ is a Heaviside step function. This can be proven by direct substitution of Eqs. (27) and (28) into Eqs. (24) and (25). The $l=1$ continuum eigenmodes are "self-shielding": there is no stream function perturbation beyond the resonant radius $r_{1,\alpha}$ because these modes do not have a dipole moment. Only the discrete $l=1$ Kelvin/diocotron mode makes a potential/stream function that can be felt at the wall; see Eq. (18). For $l>1$, however, numerical solutions for the continuum modes show that they are not perfectly self-shielding (Fig. 4); the continuum eigenmodes can all be picked up at the wall for $l>1$.

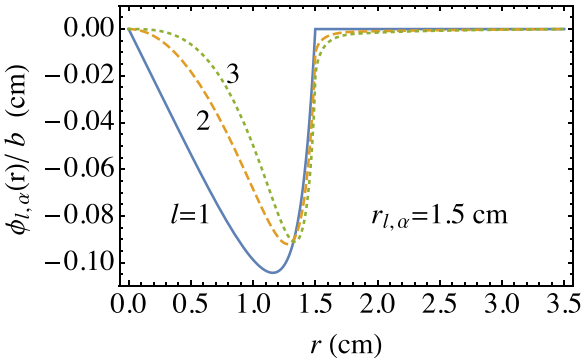

FIG. 4. Examples of the stream function $\phi_{l,\alpha}$ of continuum eigenmodes, normalized to b, for azimuthal mode numbers $l=1$, 2, 3, and for resonant radius $r_{l,\alpha}=1.5$ cm, for the vorticity profile $n_e(r)$ shown in Fig. 2.

E. Inner products, orthogonality, and completeness

It has been previously shown[11] that the vorticity eigenfunctions $n_{l,\alpha}$ form a complete orthogonal set with respect to an inner product defined as

$$\langle n_{l,\alpha}, n_{l,\beta}\rangle_P = \pi \int r^2 dr \frac{n^*_{l,\alpha} n_{l,\beta}}{\partial n_e/\partial r}. \tag{29}$$

This follows from the fact that the linear operator $\hat{L}_l$ appearing in Eq. (20) is Hermitian with respect to this inner product, so the spectral theorem applies to the eigenmodes of this operator.[11] This is a general feature of linearized non-dissipative wave systems. Due to the underlying Hamiltonian nature of the dynamics, an inner product can be found that is related to a constant of the motion, and with respect to which the system eigenmodes are orthogonal.[30] For the above inner product, the constant of the motion is the angular momentum of the mode, given by $\rho_0\langle n_{l,\alpha}, n_{l,\alpha}\rangle_P$. We will prove this in Sec. III A 2. In the plasma case, the constant of the motion associated with the above inner product is the canonical angular momentum (per unit length of the plasma column), $\frac{B^2}{4\pi c^2}\langle n_{l,\alpha}, n_{l,\alpha}\rangle_P$. We, therefore, refer to the quantity

$$P_{l,\alpha} \equiv \langle n_{l,\alpha}, n_{l,\alpha}\rangle_P \tag{30}$$

as a (scaled) angular momentum for the eigenmode.

Now, it is well known that angular momentum of a rotating wave, $P_{l,\alpha}$, is related to the wave energy $E_{l,\alpha}$, through

$$E_{l,\alpha} = \frac{\omega_{l,\alpha}}{l} P_{l,\alpha}. \tag{31}$$

Moreover, the wave energy is also related to a second inner product for the 2D Euler system,[31]

$$\langle n_{l,\alpha}, n_{l,\beta}\rangle_E = \pi \int r dr \left(n^*_{l,\alpha}\phi_{l,\beta} + \omega_e r \frac{n^*_{l,\alpha} n_{l,\beta}}{\partial n_e/\partial r}\right), \tag{32}$$

with $E_{l,\alpha} = \langle n_{l,\alpha}, n_{l,\alpha}\rangle_E$ the scaled energy, scaled in the same way as was done for the angular momentum; that is, in the Euler fluid case the actual mode energy is $\rho_0 E_{l,\alpha}$, while in the plasma analogue, the mode energy (per unit length of the plasma column) is $B^2\langle n_{l,\alpha}, n_{l,\alpha}\rangle_E/(4\pi c^2)$.

System eigenmodes are also orthogonal with respect to this energy inner product, and so

$$\langle n_{l,\alpha}, n_{l,\beta}\rangle_E = \frac{\omega_{l,\alpha}}{l}\langle n_{l,\alpha}, n_{l,\beta}\rangle_P, \tag{33}$$

for all α and β. This and other inner product relations will be derived in a following paper.[31]

Later in the paper we will need to consider a change of frame from the laboratory frame to one rotating with some angular velocity ω_ϕ. The plasma rotation frequency $\omega_e(r)$ then changes to $\bar{\omega}_e(r) = \omega_e(r) - \omega_\phi$, and eigenfrequencies are Doppler-shifted to $\bar{\omega}_{l,\alpha} = \omega_{l,\alpha} - l\omega_\phi$, but the functional form of the eigenmodes is unchanged. It then follows directly from Eqs. (30) and (31) that angular momentum and energy transform according to

$$\bar{P}_{l,\alpha} = P_{l,\alpha}, \tag{34}$$

$$\frac{\bar{E}_{l,\alpha}}{\bar{\omega}_{l,\alpha}} = \frac{E_{l,\alpha}}{\omega_{l,\alpha}}. \tag{35}$$

The latter relation is consistent with the fact that $|E_{l,\alpha}/\omega_{l,\alpha}|$ is the classical wave action (the "number of quanta" in a wave) and is, therefore, invariant under frame change.

Since wave energy is not invariant under frame change, neither is the energy inner product given by Eq. (32). Nevertheless, the eigenmodes remain orthogonal. When evaluated in a rotating frame the energy inner product is denoted by $\langle n_{l,\alpha}, n_{l,\beta}\rangle_{\bar{E}}$, given by Eq. (32) but with ω_e replaced by $\bar{\omega}_e$. On the other hand, the angular momentum inner product is frame-independent.

Completeness of the set of eigenmodes, a consequence of the Hermitian property of the operator $\hat{L}_l$, implies that any "sufficiently smooth" function $f(r)$ can be represented on $0 < r \le R$ as a superposition of the eigenmodes,

$$f(r) = \sum_\alpha c_\alpha n_{l,\alpha}(r), \tag{36}$$

while mode orthogonality implies that the "Fourier coefficients" c_α can be determined by either an energy or angular momentum inner product. Here, we will use the energy inner product defined in Eq. (32), yielding

$$c_\alpha = \frac{\langle n_{l,\alpha}, f\rangle_E}{E_{l,\alpha}}. \tag{37}$$

In Eq. (36), we have used a summation convention, appropriate for the discretized continuum modes found by using a discrete radial grid with stepsize $\Delta r = R/M$, M finite, as in Fig. 3. However, in the $M \to \infty$ continuum limit, an integral form is more appropriate. Now we split off the Kelvin/diocotron mode contribution (assuming that there is a discrete mode) and convert the remaining sum over α into an integral over the resonant radii $r_{l,\alpha}$ using Eq. (23) to relate the mode number α to a given resonant radius, obtaining

$$f(r) = \int_0^R dr_{l,\alpha} \frac{\langle n_{l,\alpha}, f\rangle_E}{\epsilon_l(r_{l,\alpha})} n_{l,\alpha}(r) + \frac{\langle n_{l,K}, f\rangle_E}{E_{l,K}} n_{l,K}(r), \tag{38}$$

where $E_{l,K}$ is the energy of the discrete Kelvin/diocotron mode, and

$$\epsilon_l(r_{l,\alpha}) \equiv \lim_{M\to\infty} \Delta r E_{l,\alpha}. \tag{39}$$

Equation (38) is a novel type of integral transform similar in some respects to an inverse Fourier transform. We will find that this transform is useful in the description of the beat wave instability considered in Sec. III.

However, there is a complication: for a continuum mode, the singularity in the mode causes a divergence such that the energy $E_{l,\alpha}$ and angular momentum $P_{l,\alpha}$ of the mode are infinite. For $l = 1$, this can be seen directly by attempting to evaluate $E_{1,\alpha}$ or $P_{1,\alpha}$ using Eqs. (27) and (28). Fortunately, we are saved by the fact that continuum mode energy enters Eq. (38) only in the combination $\epsilon_l = \lim_{M\to\infty} \Delta r E_{l,\alpha}$. When M is finite, the Dirac delta function in the continuum modes is regularized and the energy and angular momentum (found by discretizing the radial integrals in the usual way) is finite; so that Eqs. (36) and (37) are sensible equations for finite M. However in the $M \to \infty$ limit, $\Delta r \to 0$ and $E_{l,\alpha} \to \infty$ in such a way that $\epsilon_l(r_{l,\alpha})$ is a finite function.

This can be seen by direct numerical evaluation, first solving the matrix eigenvalue problem Eq. (20) on a discretized radial grid $r_j = j\Delta r$, $j = 1, \ldots, M$, with $\Delta r = R/M$, as was done for Fig. 3, and

then using these discretized eigenmodes to evaluate the eigenmode energies via a discretized version of the integral in Eq. (32). One may then use these discretized eigenmode energies to determine $\epsilon_l(r_{l,\alpha})$ via Eq. (39), and show that as M increases the result for the function $\epsilon_l(r)$ converges. However, this only provides an approximate numerical form for $\epsilon_l(r)$. An analytic approach, derived in the Appendix, yields the following exact result:

$$\epsilon_l(r_{l,\alpha}) = \pi r_{l,\alpha}^2 \omega_e(r_{l,\alpha}) \frac{b^2}{n_e'(r_{l,\alpha})} \left[1 + \left(\frac{\pi n_e'(r_{l,\alpha})\phi_{l,\alpha}(r_{l,\alpha})}{b r_{l,\alpha}\omega_e'(r_{l,\alpha})}\right)^2\right]. \quad (40)$$

We have checked that this analytic form for $\epsilon_l(r)$ agrees with the numerical approach outlined above.

III. BEAT WAVE DECAY OF A KELVIN/DIOCOTRON WAVE

In this section, we consider an experiment in which a Kelvin/diocotron "pump wave" is excited to amplitude A_p, with mode number $l_p > 1$ and frequency $\omega_p \approx \omega_{l_p,K} > 0$. This mode can decay in amplitude through a nonlinear beat wave process via the spontaneous growth of a Kelvin/diocotron mode "daughter wave" with mode number l_d in the range $0 < l_d < l_p$, frequency $\omega_d \approx \omega_{l_d,K}$, $0 < \omega_d < \omega_b$, and small but exponentially growing amplitude $A_d(t)$. In this decay process a "beat" daughter wave is also excited, with frequency $\omega_b \approx \Delta\omega \equiv \omega_{l_p,K} - \omega_{l_d,K}$, and mode number $l_b = l_p - l_d$.

The beat wave is not a discrete Kelvin/diocotron mode; otherwise this would be a standard three-wave decay process.[17] Note here that the Kelvin/diocotron mode with mode number l_b does not satisfy the three-wave resonance condition[17] $\omega_{l_p,K} = \omega_{l_d,K} + \omega_{l_b,K}$. Instead, the beat wave is the $l = l_b$ Fourier component of a discrete eigenmode of the *nonlinear* equations, drawn from a Landau-damped spectrum of continuum eigenmodes with mode number l_b.

Nevertheless, there are some similarities between beat wave decay and three-wave decay. As in three-wave decay, we will see that the daughter wave and beat wave have energies of opposite sign when viewed in the frame of the pump wave, and this allows both waves to grow through the resonant exchange of energy from the negative energy wave to the positive energy wave.[27] Also, the resonance condition $\omega_{l_p,K} = \omega_{l_d,K} + \Delta\omega$ obviously holds for the process, just as it does in three-wave decay.

A. Theory of beat wave decay

The beat wave decay process involves only a few azimuthal Fourier components: the pump wave mode number l_p, the daughter wave mode number l_d, the beat wave mode number l_b, and the complex conjugate modes $-l_p, -l_d, -l_b$. We, therefore, approximate the vorticity as

$$n(\boldsymbol{r}, t) - n_e(r) = e^{il_p\theta} n_{l_p}(r, t) + e^{il_d\theta} n_{l_d}(r, t) + e^{il_b\theta} n_{l_b}(r, t) + \text{c.c.}, \quad (41)$$

where the complex conjugate vorticity perturbations satisfy the standard Fourier identity $n_l^*(r, t) = n_{-l}(r, t)$.

We should note here that Eq. (41) neglects the nonlinear change $\delta n_0(r)$ to the $l = 0$ component of the vorticity, caused by the pump wave, as well as two other beat waves (and their complex conjugates): Fourier components $2l_p$ and $l_d + l_p$. Mode $2l_p$, the second harmonic of the pump wave, is needed to evaluate the frequency shift of the pump wave due to its finite amplitude, and mode $l_d + l_p$ is needed to evaluate an extra frequency shift term in the daughter wave and beat wave. These extra modes do not affect the growth rate of the beat wave instability at order A_p^2 and will therefore be considered separately in Sec. III A 2.

The nonlinear continuity equation for the pump wave vorticity perturbation with azimuthal mode number l_p is given by Eq. (7), after substitution of Eq. (41),

$$\frac{\partial n_{l_p}}{\partial t} + il_p\omega_e n_{l_p} + \frac{il_p\phi_{l_p}}{r}\frac{\partial n_e}{\partial r} + iF_p(r, t) = 0, \quad (42)$$

where the nonlinear term F_p is due to mode coupling to the daughter and beat waves,

$$F_p = l_b\left(\frac{\phi_{l_b}}{r}\frac{\partial n_{l_d}}{\partial r} - \frac{n_{l_b}}{r}\frac{\partial \phi_{l_d}}{\partial r}\right) + l_d\left(\frac{\phi_{l_d}}{r}\frac{\partial n_{l_b}}{\partial r} - \frac{n_{l_d}}{r}\frac{\partial \phi_{l_b}}{\partial r}\right). \quad (43)$$

However, we will assume for simplicity that the daughter wave and beat wave are much smaller in amplitude than the pump wave so we drop F_p. This linearizes the equation, and along with the Poisson equation (8) yields a linear Kelvin/diocotron mode solution for $n_{l_p}(r, t)$,

$$n_{l_p} = A_p e^{-i\omega_{l,K}t} n_{l,K}(r), \quad (44)$$

where A_p is the dimensionless mode amplitude of the Kelvin/diocotron mode; see Eqs. (16), (17), and (19). Dropping F_p implies that the pump wave has time-independent amplitude A_p; this is a good approximation only in the early stages of growth of the daughter and beat waves, before they grow large enough to noticeably deplete the pump wave, but this is enough to determine the growth rate of the instability.

Here, and throughout the paper, we use the normalization convention that discrete Kelvin/diocotron eigenmodes $n_{l,K}(r)$ are real with dimensionless amplitudes [defined by Eq. (19)] equal to unity. For simplicity, we also assume that A_p is real.

For the daughter and beat waves, we will work in the frame of the pump wave, which rotates at phase velocity $\omega_\phi = \omega_{l_p,K}/l_p$ with respect to the lab frame. This greatly simplifies the analysis because the pump wave is stationary in this frame, with stream function $2A_p\phi_{l,K}(r)\cos(l_p\theta)$ (after adding in the complex conjugate mode). This allows a description of the daughter and beat waves in terms of an eigenmode of a new equilibrium that includes the stationary pump wave perturbation. Nonlinear coupling between the daughter wave, beat wave, and the pump wave can then be understood in terms of a fairly straightforward perturbation theory of the eigenfrequencies of the new equilibrium.

The equation for the $l = l_b$ beat wave vorticity perturbation $n_{l_b}(r)$ is also given by Eq. (7),

$$\frac{\partial n_{l_b}}{\partial t} + il_b\bar{\omega}_e n_{l_b} + \frac{il_b\phi_{l_b}}{r}\frac{\partial n_e}{\partial r} + iA_pF_b(r, t) = 0, \quad (45)$$

where $\bar{\omega}_e = \omega_e - \omega_\phi$ is the rotation frequency as seen in the rotating frame of the pump wave, and the nonlinear term $F_b(r, t)$ is due to mode coupling to the pump wave and the $l = -l_d$ Fourier component of the daughter wave,

$$F_b(r,t) = -l_d\left(\frac{\phi_{-l_d}(r,t)}{r}\frac{\partial n_{l_p,K}}{\partial r} - \frac{n_{-l_d}(r,t)}{r}\frac{\partial \phi_{l_p,K}}{\partial r}\right) + l_p\left(\frac{\phi_{l_p,K}}{r}\frac{\partial n_{-l_d}}{\partial r}(r,t) - \frac{n_{l_p,K}}{r}\frac{\partial \phi_{-l_d}}{\partial r}(r,t)\right). \quad (46)$$

Next, we write a similar equation for the daughter wave Fourier component $-l_d$, since this is the component that appears in Eq. (46):

$$\frac{\partial n_{-l_d}}{\partial t} - il_d\bar{\omega}_e n_{-l_d} - \frac{il_d\phi_{-l_d}}{r}\frac{\partial n_e}{\partial r} + iA_pF_d(r,t) = 0, \quad (47)$$

where the nonlinear term $F_d(r,t)$ is due to mode coupling between the $l = l_b$ Fourier component of the beat wave and the $l = -l_p$ component of the pump wave,

$$F_d(r,t) = l_b\left(\frac{\phi_{l_b}(r,t)}{r}\frac{\partial n_{l_p,K}}{\partial r} - \frac{n_{l_b}(r,t)}{r}\frac{\partial \phi_{l_p,K}}{\partial r}\right) - l_p\left(\frac{\phi_{l_p,K}}{r}\frac{\partial n_{l_b}}{\partial r}(r,t) - \frac{n_{l_p,K}}{r}\frac{\partial \phi_{l_b}}{\partial r}(r,t)\right), \quad (48)$$

and where we used the fact that $n_{l_p,K}(r)$ is real, so that $n_{-l_p,K} = n_{l_p,K}$, and similarly for $\phi_{l_p,K}$.

We expect that Fourier component $-l_d$ is close to a discrete Kelvin/diocotron mode with vorticity eigenmode $n_{l_d,K}(r)$, stream function eigenmode $\phi_{l_d,K}$, and some growing amplitude $a_{-l_d}(t) = a^*_{l_d}(t)$, so we write the solution to Eq. (47) as

$$\begin{aligned} n_{-l_d}(r,t) &= a^*_{l_d}(t)n_{l_d,K}(r) + \Delta n(r,t), \\ \phi_{-l_d}(r,t) &= a^*_{l_d}(t)\phi_{l_d,K}(r) + \Delta\phi(r,t), \end{aligned} \quad (49)$$

where $\Delta n(r,t)$ and $\Delta\phi$ are small corrections. Recall that the Kelvin/diocotron eigenmode is chosen so that $n_{l_d,K}$ and $\phi_{l_d,K}$ are real, so that $n_{-l_d,K} = n_{l_d,K}$ and $\phi_{-l_d,K} = \phi_{l_d,K}$. However, a_{l_d} may be complex, describing an arbitrary phase shift between the Kelvin/diocotron daughter wave and the pump wave. The corrections Δn and $\Delta\phi$ can be expressed as a sum (integral) over the other continuum eigenmodes of azimuthal mode number $-l_d$. By construction, Δn is orthogonal to $n_{l_d,K}$, with orthogonality defined by either of the inner products discussed in Sec. II E.

Applying Eq. (49) to Eq. (47) then yields

$$\dot{a}^*_{l_d}n_{l_d,K} + \Delta\dot{n} + i\hat{\bar{L}}_{-l_d}(a^*_{l_d}n_{l_d,K} + \Delta n) + iA_pF_d = 0, \quad (50)$$

where $\hat{\bar{L}}_{l_p}$ is the linear Kelvin/diocotron eigenmode operator of Eq. (20) as viewed in the rotating frame of the pump wave,

$$\hat{\bar{L}}_{l_p}n_{l_p} = l\bar{\omega}_e n_{l_p} + \frac{l}{r}\frac{\partial n_e}{\partial r}\hat{G}n_{l_p}. \quad (51)$$

We simplify Eq. (50) by taking an energy inner product with respect to the Kelvin/diocotron eigenmode $n_{l_d,K}$ to obtain the following evolution equation for the dimensionless Kelvin/diocotron mode amplitude $a_{l_d}(t)$, as viewed in the frame of the pump wave,

$$\bar{E}_{l_d,K}(\dot{a}^*_{l_d} + i\bar{\omega}_{-l_d,K}a^*_{l_d}) + \langle n_{l_d,K}, iA_pF_d\rangle_{\bar{E}} = 0, \quad (52)$$

where $\bar{\omega}_{-l_d,K} = -\bar{\omega}_{l_d,K}$ is the Doppler-shifted frequency of the $-l_d$ Kelvin/diocotron eigenmode, as seen in the pump wave frame, and $\bar{E}_{l_d,K} = \langle n_{l_d,K}, n_{l_d,K}\rangle_{\bar{E}}$ is the energy of an $l = l_d$ or $-l_d$ Kelvin/diocotron eigenmode as seen in the pump wave frame.

Turning to the beat wave with mode number l_b, we substitute for n_{-l_d} and ϕ_{-l_d} into F_b from Eq. (49), and drop the small corrections Δn and $\Delta\phi$ since the F_b term in Eq. (45) is already small. This yields

$$\dot{n}_{l_b} + il_b\bar{\omega}_e n_{l_b} + \frac{il_b\phi_{l_b}}{r}\frac{\partial n_e}{\partial r} + iA_pa^*_{l_d}(t)F_{b,K}(r) = 0, \quad (53)$$

where the beat wave forcing function $F_{b,K}$ is determined entirely by the Kelvin/diocotron mode densities and stream functions,

$$F_{b,K}(r) = -l_d\left(\frac{\phi_{l_d,K}}{r}\frac{\partial n_{l_p,K}}{\partial r} - \frac{n_{l_d,K}}{r}\frac{\partial \phi_{l_p,K}}{\partial r}\right) + l_p\left(\frac{\phi_{l_p,K}}{r}\frac{\partial n_{l_d,K}}{\partial r} - \frac{n_{l_p,K}}{r}\frac{\partial \phi_{l_d,K}}{\partial r}\right). \quad (54)$$

Equations (52) and (53) are coupled linear homogeneous differential equations with time-independent coefficients, so solutions with time-dependence of the form $\exp(-i\bar{\omega}t)$ exist,

$$(a^*_{l_d}(t), n_{l_b}(r,t)) = e^{-i\bar{\omega}t}(A^*_{di}, \tilde{n}_{l_b}(r)), \quad (55)$$

where A_{di} is the dimensionless initial amplitude of the l_d diocotron mode and $\tilde{n}_{l_b}(r)$ is the radial dependence of the beat wave.

Equations (52) and (53) can then be expressed as

$$\bar{\omega}A^*_{di} = \bar{\omega}_{-l_d,K}A^*_{di} + A_p\frac{\langle n_{l_d,K}, \tilde{F}_d\rangle_{\bar{E}}}{\bar{E}_{l_d,K}}, \quad (56)$$

$$\bar{\omega}\tilde{n}_{l_b}(r) = l_b\bar{\omega}_e\tilde{n}_{l_b}(r) + \frac{l_bn'_e(r)}{r}\tilde{\phi}_{l_b}(r) + A_pA^*_{di}F_{b,K}(r), \quad (57)$$

where $\tilde{\phi}_{l_b}(r) = e^{i\bar{\omega}t}\phi_{l_b}(r,t)$ and $\tilde{F}_d(r) = e^{i\bar{\omega}t}F_d(r,t)$. These coupled equations are an eigenvalue problem for the daughter and beat wave vector eigenfunction $(A^*_{di}, \tilde{n}_{l_b}(r))$, if we recall that F_d is linear in n_{l_b} and ϕ_{l_b}, and that $\phi_{l_b} = \hat{G}_{l_b}n_{l_b}$. This eigenvalue problem includes the mode-coupling effect of the pump wave on the daughter and beat waves, and can therefore describe the nonlinear beat wave instability.

These eigenvalue equations can be solved numerically by discretizing radius, and then determining the eigenvalues and eigenvectors of the resulting matrix eigenvalue problem. This is a simple generalization of the numerical method used to find linear continuum eigenmodes of the unperturbed ($A_p = 0$) system discussed in relation to Fig. 3. We will use this numerical method later, but for now, we will obtain analytic expressions for the instability growth rate and frequency shift.

In the beat wave decay process, the $l = l_b$ perturbation is a wavepacket of continuum modes, so we write the vorticity perturbation as

$$\tilde{n}_{l_b}(r) = \sum_\alpha a_\alpha n_{l_b,\alpha}(r), \quad (58)$$

where the sum is over all of the $l = l_b$ continuum eigenmodes as well as the single discrete $l = l_b$ Kelvin/diocotron eigenmode. We will later convert the sum over continuum eigenmodes into an integral, but for now it is convenient to leave the expression in this form. Using this eigenmode expansion in Eq. (57) and taking an energy inner product with respect to one eigenmode then yield

$$\bar{E}_{l_b,\alpha}\bar{\omega}a_\alpha = \bar{E}_{l_b,\alpha}\bar{\omega}_{l_b,\alpha}a_\alpha + A_pA^*_{di}C_{\alpha d}, \quad (59)$$

where the nonlinear coupling coefficient $C_{\alpha d}$ between the continuum eigenmode and the daughter wave is defined as

$$C_{\alpha d} \equiv \langle n_{l_b,\alpha}, F_{b,K} \rangle_{\bar{E}}. \tag{60}$$

On the other hand, in Eq. (56) $\tilde{F}_d = e^{i\bar{\omega}t} F_d$ depends on n_{l_b} and ϕ_{l_b}; see Eq. (48). Substituting for $n_{l_b} = e^{-i\bar{\omega}t}\tilde{n}_{l_b}$ and $\phi_{l_b} = e^{-i\bar{\omega}t}\phi_{l_b}$ in terms of the eigenmode expansion via Eq. (58), Eq. (56) then becomes

$$\bar{\omega} A^*_{di} = \bar{\omega}_{-l_d,K} A^*_{di} + A_p \sum_\alpha C_{d\alpha} a_\alpha = 0, \tag{61}$$

where the second nonlinear coupling coefficient $C_{d\alpha}$ between the continuum mode and the daughter wave is defined as

$$C_{d\alpha} \equiv \langle n_{l_d,K}, F_{d,\alpha} \rangle_{\bar{E}}, \tag{62}$$

and where

$$F_{d,\alpha}(r) = \frac{l_b}{r}(\phi_{l_b,\alpha} n'_{l_p,K} - n_{l_b,\alpha}\phi'_{l_p,K}) - \frac{l_p}{r}(\phi_{l_p,K} n'_{l_b,\alpha} - n_{l_p,K}\phi'_{l_b,\alpha}), \tag{63}$$

Equations (59) and (61) are coupled linear equations for daughter wave amplitude A^*_{di} and continuum mode amplitude a_α. The equations can be solved to obtain the frequency and growth rate of the decay instability. First, one can solve Eq. (59) for a_α in terms of A^*_{di}. Substituting the result into Eq. (61) yields

$$D(\bar{\omega}) A^*_{di} = 0, \tag{64}$$

where $D(\bar{\omega})$, the nonlinear dielectric function, is

$$D(\bar{\omega}) = \bar{\omega} - \bar{\omega}_{-l_d,K} - A_p^2 \sum_\alpha \frac{C_{d\alpha} C_{\alpha d}}{\bar{E}_{l_b,\alpha}\bar{E}_{l_d,K}(\bar{\omega} - \bar{\omega}_{l_b,\alpha})}. \tag{65}$$

To evaluate the sum appearing in this expression, we now separate the single Kelvin/diocotron mode contribution, with frequency $\bar{\omega}_{l_b,K} = \omega_{l_b,K} - l_b\omega_\phi$ in the pump wave frame, energy $\bar{E}_{l_b,K}$, and coupling coefficients C_{dK}, C_{Kd} [obtained by replacing α by K in Eqs. (60), (62), and (63)]. We convert the rest of the sum to an integral since we are dealing with continuum modes. Following the discussion surrounding Eq. (38) we obtain

$$D(\bar{\omega}) = \bar{\omega} - \bar{\omega}_{-l_d,K} - A_p^2 \frac{C_{dK} C_{Kd}}{\bar{E}_{l_b,K}\bar{E}_{l_d,K}(\bar{\omega} - \bar{\omega}_{l_b,K})} - A_p^2 \int dr_\alpha \frac{C_{d\alpha} C_{\alpha d}}{\bar{\epsilon}_{l_b}(r_\alpha)\bar{E}_{l_d,K}(\bar{\omega} - l_b\bar{\omega}_e(r_\alpha))}, \tag{66}$$

where $\bar{\epsilon}_l(r_\alpha)$ is given by Eq. (40), evaluated in the barred (pump wave) frame.

We search for a zero of the dielectric function. Anticipating that for small A_p, $\bar{\omega} \approx \bar{\omega}_{-l_d,K} + i\gamma$ for some growth rate γ (assumed small), we use this in the $0(A_p^2)$ terms to obtain a perturbed value for $\bar{\omega}$,

$$D(\bar{\omega}) = 0 = \bar{\omega} - \bar{\omega}_{-l_d,K} - A_p^2 \frac{C_{dK} C_{Kd}}{\bar{E}_{l_b,K}\bar{E}_{l_d,K}(\bar{\omega}_{-l_d,K} - \bar{\omega}_{l_b,K})} - A_p^2 \int dr_\alpha \frac{C_{d\alpha} C_{\alpha d}}{\bar{\epsilon}_{l_b}(r_\alpha)\bar{E}_{l_d,K}(\bar{\omega}_{-l_d,K} + i\gamma - l_b\bar{\omega}_e(r_\alpha))}. \tag{67}$$

We apply the Plemelj formula to the Landau pole in the last integral and solve for $\bar{\omega}$, yielding

$$\bar{\omega} = \bar{\omega}_{-l_d,K} + \delta\omega + i\gamma, \tag{68}$$

where the growth rate γ and nonlinear frequency shift $\delta\omega$ are

$$\gamma = -\pi A_p^2 \int dr_\alpha \frac{C_{d\alpha} C_{\alpha d}}{\bar{\epsilon}_{l_b}(r_\alpha)\bar{E}_{l_d,K}} \delta(l_b\bar{\omega}_e(r_\alpha) - \bar{\omega}_{-l_d,K}), \tag{69}$$

$$\delta\omega = A_p^2 \mathcal{P} \int dr_\alpha \frac{C_{d\alpha} C_{\alpha d}}{\bar{\epsilon}_{l_b}(r_\alpha)\bar{E}_{l_d,K}(\bar{\omega}_{-l_d,K} - l_b\bar{\omega}_e(r_\alpha))} + A_p^2 \frac{C_{dK} C_{Kd}}{\bar{E}_{l_b,K}\bar{E}_{l_d,K}(\bar{\omega}_{-l_d,K} - \bar{\omega}_{l_b,K})}, \tag{70}$$

and where $\mathcal{P}$ is the Cauchy principal value of the integral.

The expression for the growth rate γ involves a Dirac delta function, which is nonzero only when the resonance condition $\bar{\omega}_{-l_d,K} = l_b\bar{\omega}_e(r_\alpha) = \bar{\omega}_{l_b,\alpha}$ is met, i.e., the daughter and beat waves have the same frequency when viewed in the frame of the pump wave. The resonance condition is met at a radial location $r_\alpha = r_{beat}$, the beat wave resonant radius. Transforming the resonance condition to the lab frame yields a more familiar form for the resonance condition,

$$\omega_{l_b,\alpha} = l_b\omega_e(r_{beat}) = \omega_{l_p,K} - \omega_{l_d,K} = \Delta\omega. \tag{71}$$

This Landau resonance at the beat frequency $\Delta\omega$ between the Kelvin/diocotron modes occurs at a location within the plasma where both $\partial n_e/\partial r$ and $F_{b,K}$ are typically nonzero: see Fig. 2.

At such a resonance, energy conservation for the daughter and beat waves then implies $C_{\alpha d} = C^*_{d\alpha}$.[31] This can be verified by direct calculation of $C_{\alpha d}$ and $C_{d\alpha}$. Therefore, we may write

$$\gamma = -\pi A_p^2 \int dr_\alpha \frac{|C_{\alpha d}|^2}{\bar{\epsilon}_{l_b}(r_\alpha)\bar{E}_{l_d,K}} \delta(l_b\bar{\omega}_e(r_\alpha) - \bar{\omega}_{-l_d,K}) \tag{72}$$

$$= -\pi A_p^2 \frac{|C_{\alpha d}|^2}{|l_b\bar{\omega}'_e(r_\alpha)|\bar{\epsilon}_{l_b}(r_\alpha)\bar{E}_{l_d,K}}|_{r_\alpha = r_{beat}}. \tag{73}$$

Note that $\bar{\epsilon}^{-1}_{l_b}(r_{beat}) \propto n'_e(r_{beat})$ [see Eq. (40)], so the growth rate is nonzero only if there is a nonzero equilibrium vorticity gradient at the beat wave resonant radius.

Also, the growth rate is positive only when the beat and daughter wave energies in the pump wave frame are of opposite sign, satisfying $\bar{\epsilon}_{l_b}\bar{E}_{l_d,K} < 0$. This is consistent with a general criterion for instability due to mode coupling between two daughter waves:[19,27] when the waves have equal frequencies and energies of opposite sign when viewed in the frame of the pump wave, the negative energy daughter wave can then resonantly transfer energy to the positive energy wave, allowing both daughter waves to grow.

In the lab frame, all two-dimensional drift waves have negative energy, including the $l = -l_d$ Kelvin/diocotron wave and the $l = l_b$ beat wave. Note, however, that their lab frame frequencies are of opposite sign, since $\omega_{-l_d,K} = -\omega_{l_d,K} < 0$ but $\omega_{l_b,\alpha} = \Delta\omega > 0$. However, in the pump wave frame their frequencies are the same, $\bar{\omega}_{l_b,\alpha} = \bar{\omega}_{-l_d,K} > 0$. This implies, via Eq. (35), that the daughter wave energies are of opposite sign when viewed in the pump wave frame, satisfying the instability criterion. In the pump wave frame, the $l = l_d$ Kelvin/diocotron mode has positive energy, while the $l = l_b$ beat wave has negative energy. Thus, when viewed in this frame, energy flows from the negative energy beat wave to the positive energy Kelvin/diocotron wave, so that both grow. The energy is extracted from the wave-packet of resonant $l = l_b$ continuum modes making up the beat wave, a Landau damping process that induces wave growth rather than damping due to the resonant interaction with the positive energy daughter wave.

Equation (73) is similar in some respects to Eq. (10) of Ref. 13, although we have not been able to determine whether the expressions yield the same growth rate. Rather than a sum over wavenumbers involving an inverse propagator that appears in Ref. 13, our expression for the growth rate involves a single resonant continuum mode—in the eigenmode expansion, the propagator is analytically invertible as an eigenmode frequency, which simplifies the growth rate expression.

Equation (73) implies that the growth rate is proportional to the *square* of the pump wave amplitude A_p. The A_p^2 scaling of the growth rate with pump amplitude is one of the main observations in past experiments on beat wave decay.[14] However, by neglecting higher harmonics of l_p in Eq. (41), we are treating the pump wave as a linear mode, which is only a good approximation for small pump amplitudes A_p. Our expression for the growth rate is therefore valid only to lowest order in A_p.

The growth rate expression, Eq. (73), is fairly easy to evaluate since only a single continuum eigenmode is required: the mode at the beat wave frequency, i.e., $\omega_{l_b,\alpha} = \Delta\omega$. For $l_b = 1$ the mode is known analytically [Eqs. (27) and (28)], while for $l_b > 1$ it can be evaluated via the numerical methods discussed in Sec. II. One such method uses the discretized version of the resonant continuum mode obtained for finite Δr, along with discretized forms for the inner products $C_{\alpha d}, \bar{E}_{l_b,\alpha}$ involving this mode. When these inner products are written in terms of sums, each sum is proportional to Δr. In the denominator, $\bar{\epsilon}_l = \Delta r \bar{E}_{l_b,\alpha} \propto \Delta r^2$ and this factor of Δr^2 cancels with the same factor arising from $|C_{\alpha d}|^2$ in the numerator, leaving a finite result for γ that approaches the continuum limit as $\Delta r \to 0$, *provided that* Δr is chosen so that the resonant radius of the beat wave, r_{beat}, is on the grid, i.e., $r_{beat}/\Delta r \in$ Integers. More accurate numerical results can be obtained by evaluating the inner products in Eq. (73) using the resonant continuum mode obtained from a high accuracy shooting method solution of Eq. (25), or via the Green's function approach of Eq. (26).

1. Alternate expressions

The expressions developed so far for the frequency shift $\delta\omega$ and the functional form of the beat wave, as integrals over the continuum eigenmodes, are unwieldy. More elegant, easy to evaluate expressions can be found. We return to eigenvalue equations (56) and (57) for the initial Kelvin/diocotron amplitude A_{di}^* and the beat wave vorticity $\tilde{n}_{l_b}(r)$. Noting that the eigenfrequency $\bar{\omega} \approx \bar{\omega}_{-l_d,K} + i\gamma$, we will use this approximate expression to determine alternate forms for the real frequency shift, the growth rate, and the radial dependence of the beat wave vorticity perturbation, without employing a continuum mode expansion.

We first define and the scaled beat wave vorticity and stream function,

$$\hat{n}_{l_b}(r) \equiv \tilde{n}_{l_b}(r)/(A_p A_{di}^*), \quad \hat{\phi}_{l_b}(r) \equiv \tilde{\phi}_{l_b}(r)/(A_p A_{di}^*), \tag{74}$$

and then solve Eq. (57) for $\hat{n}_{l_b}$ and apply the Plemelj formula (assuming γ is small), yielding

$$\hat{n}_{l_b} = \left(\frac{l_b}{r}\hat{\phi}_{l_b}\frac{\partial n_e}{\partial r} + F_{b,K}\right)\left(\frac{P}{\bar{\omega}_{-l_d,K} - l_b\bar{\omega}_e} - i\pi\delta(\bar{\omega}_{-l_d,K} - l_b\bar{\omega}_e)\right). \tag{75}$$

Combining this with Poisson's equation yields an inhomogeneous boundary value problem for the scaled beat wave stream function $\hat{\phi}_{l_b}(r)$,

$$\frac{\partial^2\hat{\phi}_{l_b}}{\partial r^2} + \frac{1}{r}\frac{\partial\hat{\phi}_{l_b}}{\partial r} - \frac{l_b^2}{r^2}\hat{\phi}_{l_b} + \hat{n}_{l_b} = 0 \tag{76}$$

with boundary condition $\hat{\phi}_{l_b}(r_w) = 0$.

The inhomogeneous term in Eq. (75), proportional to $F_{b,K}(r)$, drives the beat wave stream function. Furthermore, the function $\tilde{F}_d(r) = e^{i\bar{\omega}t}F_d(r,t)$ appearing in the inner product in Eq. (56) is linear in $\tilde{n}_{l_b}(r)$ and $\tilde{\phi}_{l_b}(r)$, [see Eq. (48)], and so $\tilde{F}_d$ is also proportional to $A_p A_{di}^*$. This implies that we can divide out a factor of A_{di}^* from every term in Eq. (56), leaving the expression

$$\bar{\omega} = \bar{\omega}_{-l_d,K} + A_p^2\frac{\langle n_{2,K}, \hat{F}_d\rangle_{\bar{E}}}{\bar{E}_{l_d,K}}, \tag{77}$$

where

$$\hat{F}_d(r) \equiv \frac{\tilde{F}_d(r)}{A_p A_{di}^*} = \frac{l_b}{r}(\hat{\phi}_{l_b}n'_{l_p,K} - \hat{n}_{l_b}\phi'_{l_p,K}) - \frac{l_p}{r}(\phi_{l_p,K}\hat{n}'_{l_b} - n_{l_p,K}\hat{\phi}'_{l_b}). \tag{78}$$

Equation (77) is an alternate expression for the growth rate and real frequency shift in the beat wave instability, which can be evaluated without needing to evaluate and integrate over the continuum eigenmodes. Instead, the inner product involves the scaled beat wave vorticity and stream function $\hat{n}_{l_b}$ and $\hat{\phi}_{l_b}$. It can be written explicitly in a fairly compact form as an integral over these functions by converting the energy inner product to an angular momentum inner product using Eqs. (33) and (31) and then applying Eq. (29), yielding

$$\bar{\omega} - \bar{\omega}_{-l_d,K} = \delta\omega + i\gamma = -\frac{\pi A_p^2}{P_{l_d,K}}\int dr\Big[\hat{n}_{l_b}(l_d r r_{l_d}\phi'_{l_p,K} + l_p(r r_{l_d})'\phi_{l_p,K}) - \hat{\phi}_{l_b}(l_d r r_{l_d}n'_{l_p,K} + l_p(r r_{l_d})'n_{l_p,K})\Big], \tag{79}$$

where we introduce $r_l(r) \equiv -n_{l,K}/n'_e$, the radial displacement of fluid elements in a Kelvin/diocotron eigenmode, and where we have combined terms after substituting $l_b = l_p - l_d$ and integrating by parts, so that no radial derivatives of $\hat{n}_{l_b}$ or $\hat{\phi}_{l_b}$ appear.

This expression shows that the real parts of the scaled beat wave vorticity $\hat{n}_{l_b}$ and stream function $\hat{\phi}_{l_b}$ are responsible for the frequency shift $\delta\omega$, and the imaginary parts determine the growth rate γ. The real parts of the beat wave are in phase with the l_d Kelvin/diocotron mode, and the imaginary parts are 90° out of phase (when viewed in the pump frame where the daughter and beat waves have the same frequency). As is typically the case, growth (or damping) of waves due to interaction between them requires a phase shift between the waves.

In the Appendix, it is shown that the imaginary part of the beat wave vorticity is directly proportional to the resonant continuum eigenmode $n_{l_b,\alpha}$ that enters our previous expression for the growth rate, Eq. (72), so Eqs. (79) and (72) yield the same result for γ.

As a special case, Eq. (79) simplifies when the daughter wave is assumed to have mode number $l_d = 1$. Mathematically, this is due to a cancelation between the term in the integrand proportional to $\hat{\phi}_{l_b}$ and

the term proportional to $\hat{n}_{l_b}$, which occurs because r_{l_d} = constant for the $l_d = 1$ Kelvin/diocotron mode: the mode is a uniform displacement of the plasma off of the trap axis. The cancelation is then proven by performing two integrations by parts on the $\hat{n}_{l_b}$ term after substituting from Poisson equation (76) for $\hat{n}_{l_b}$ in terms of $\hat{\phi}_{l_b}$, then substituting for $\phi''_{l_p,K}$ and $\phi'''_{l_p,K}$ in terms of $n_{l_p,K}$ and $n'_{l_p,K}$ respectively, and then taking $l_d = 1$ and $l_p = 1 + l_b$. After the cancelations a single boundary value term is left over from the integrations by parts, yielding

$$\delta\omega + i\gamma = \frac{\pi A_p^2}{P_{l_d,K}} r_w r_{l_d} \hat{\phi}'_{l_b}(r_w)\phi'_{l_p,K}(r_w), \quad \text{if } l_d = 1. \tag{80}$$

Thus, for $l_d = 1$, instability arises from the imaginary part of the beat wave electric field [proportional to $\hat{\phi}'_{l_b}(r)$] evaluated at the wall radius r_w. If the wall is very far away, $r_w \to \infty$, the growth rate therefore vanishes. Intuitively, this makes sense because in the absence of a wall, the location of the center of mass of the plasma column (the "center of vorticity" of the fluid vortex) is a constant of the motion, and so in this case the $l_d = 1$ Kelvin/diocotron mode, which is a displacement of the center of vorticity, cannot be spontaneously excited by coupling to other vortex modes.

Evaluation of Eq. (79) [or Eq. (80)] requires an accurate functional form for the beat wave stream function $\hat{\phi}_{l_b}$. For $l_b = 1$, we will see in a moment that an analytic form for this function can be found. For $l_b > 1$, however, the inhomogeneous boundary value problem given by Eqs. (75) and (76) must be solved numerically. There are several ways of doing so. We have found that the most accurate and efficient approach is to use a shooting method in which, for $\hat{\phi}_{l_b}(0) = 0$ and an arbitrary value of $\hat{\phi}'_{l_b}(0)$, a numerical solution is obtained in the range $0 < r < r_{beat} - \epsilon$, for some $\epsilon \ll 1$; a typical value is $\epsilon = 10^{-4}$. This solution is then connected across the resonance to an outer numerical solution running from $r_{beat} + \epsilon$ to r_w, using an analytic power series solution in the connection region $|r - r_{beat}| < \epsilon$ of the form $\hat{\phi}_{l_b}(r_{beat} + x) = a_0 + \sum_{m=1}^{M} x^m(a_m + b_m \log|x|)$, where the series coefficients (a_m, b_m) are related to (a_{m-1}, b_{m-1}) through a recursion relation. Note that the coefficient a_1 changes value from $x < 0$ to $x > 0$ in order to account for the delta function in n_{l_b}, and this changes the other coefficients through the recursion relation. Then, $\hat{\phi}'_{l_b}(0)$ is varied until the boundary condition $\hat{\phi}_{l_b}(r_w) = 0$ is obtained in the outer solution.

For the case $l_b = 1$, (the case observed in previous experiments[14]) the boundary value problem for $\hat{\phi}_{l_b}$, Eqs. (75) and (76), is solvable analytically for general equilibrium vorticity profiles. The imaginary parts of $\hat{\phi}_{l_b}$ and $\hat{n}_{l_b}$, $\hat{\phi}_i$ and $\hat{n}_i$, respectively, are particularly simple:

$$\hat{\phi}_i = \frac{D}{\omega'_e(r_{beat})} \begin{cases} r(\Delta\omega - \omega_e(r)), & r < r_{beat}, \\ 0, & r \geq r_{beat}, \end{cases} \tag{81}$$

where the coefficient D (with units of vorticity) is given by

$$D = \frac{\pi}{r_{beat}^2 |\omega'_E(r_{beat})|}(\hat{\phi}_r(r_{beat})n'_e(r_{beat}) + r_{beat}F_{b,K}(r_{beat})), \tag{82}$$

and where the real part of $\hat{\phi}_{l_b}$ when evaluated at the Landau resonance radius r_{beat}, is given by the expression

$$\hat{\phi}_r(r_{beat}) = -\frac{1}{r_{beat}^2 \omega'_E(r_{beat})} \int_0^{r_{beat}} dr r^2 F_{b,K}(r). \tag{83}$$

The imaginary part of the vorticity is then found by taking the imaginary part of Eq. (75), yielding

$$\hat{n}_i(r) = D\left[\frac{n'_e(r)}{\omega'_e(r_{beat})} h(r_{beat} - r) - r_{beat}\delta(r - r_{beat})\right], \tag{84}$$

where $h(x)$ is the Heaviside step function.

The real parts of the vorticity and stream function can also be found in integral form. The real part of the stream function, $\hat{\phi}_r$, is

$$\hat{\phi}_r(r) = -\psi_b(r)\int_0^r r'^2 dr' F_{b,K}(r') - \psi_a(r)\mathcal{P}\int_r^{r_w} r'^2 dr' \frac{\psi_b(r')F_{b,K}(r')}{\psi_a(r')}, \tag{85}$$

where the functions ψ_a and ψ_b are $l = 1$ homogeneous solutions to the differential equation appearing in Eq. (25),

$$\psi_a(r) = r(\Delta\omega - \omega_e(r)), \tag{86}$$

$$\psi_b(r) = -\psi_a(r)\oint_r^{r_w} \frac{dr'}{r'\psi_a(r')^2}, \tag{87}$$

and where here C is any contour in the complex r' plane running from r to r_w that avoids the pole at $r' = r_{beat}$ [note that $\psi_a(r_{beat}) = 0$]. The real part of the beat wave vorticity is then

$$\hat{n}_r = \frac{P}{\psi_a}(n'_e\hat{\phi}_r + rF_{b,K}), \tag{88}$$

where P stands for the principal part of the resonant denominator.

In Fig. 5, the complex beat wave stream function $\hat{\phi}_{l_b}$ is plotted vs radius for the $3 \to 2$ decay, i.e., for $l_b = 1, l_d = 2, l_p = 3$. The beat wave stream function is calculated for the same vorticity profile as shown in Fig. 2. The figure shows that there is a discontinuity in slope of the imaginary part of the stream function at the beat wave resonant radius r_{beat} [see also Eq. (81) which describes this analytically for $l_b = 1$)], and a "jog" in the real part, which has logarithmically infinite slope (i.e., an infinite velocity field) at the resonance.

The inset to the figure shows that the beat wave stream function is almost, but not quite, self-shielding: there is a weak beat wave velocity field at the wall. The corresponding electric field at the wall in the plasma analogue, in the lab frame, is, in principle at least, a measurable quantity in the plasma experiments, given by the expression $E_{l_b}(r_w, t) = -e^{-i(\bar{\omega}+l_b\omega_\phi)t}\partial\Phi_{l_b}(r)/\partial r|_{r_w}$ with $\Phi_{l_b}(r) = \pm B\hat{\phi}_{l_b}(r)/c$ [with the upper (lower) sign for positive (negative) nonneutral

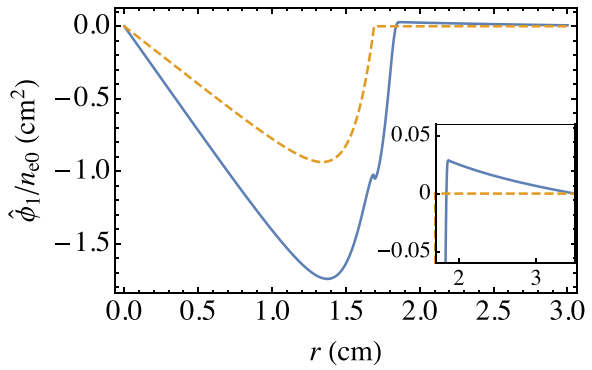

FIG. 5. Real (solid) and imaginary (dashed) components of the radial dependence $\hat{\phi}_{l_b}(r)$ of the beat wave stream function $\phi_{l_b}(r,t) = A_p A_{dl}^* e^{-i\bar{\omega}t}\hat{\phi}_{l_b}(r)$ for a $3 \to 2$ decay, assuming infinitesimal pump wave amplitude A_p.

plasmas]. For $l_b = 1$, the beat wave electric field at the wall can then be determined analytically from Eqs. (85)–(87):

$$E_1(r_w,t) = \pm\frac{B}{c\,r_w\psi_a(r_w)}A_pA_{di}^*\exp\left(-i(\bar{\omega}+\omega_\phi)t\right)\int_0^{r_w} r^2 dr F_{b,K}(r), \tag{89}$$

where we also used Eqs. (55) and (74).

For $l_b = 1$, Eq. (89) shows that the beat wave electric field is proportional to the dipole moment of the beat wave forcing function $F_{b,K}$. For the $3 \to 2$ decay, the ratio of the wall electric fields of the beat wave to the l_d daughter wave is fairly small, given by $0.07A_p$, so the beat wave field is difficult to observe in the experiments for this decay.

In Fig. 6, the complex beat wave vorticity n_{l_b} for the $3 \to 2$ decay is plotted vs radius. The vorticity is singular at the resonant radius r_{beat}. The singularities in the beat wave vorticity and stream function are expected because the beat wave has a Landau resonance. For growth rate $\gamma \to 0$ (i.e., for pump amplitude $A_p \to 0$), the imaginary part of the beat wave is proportional to a single singular continuum eigenmode, as discussed in the Appendix, see Eq. (A8). However, for finite growth rate γ (i.e., finite pump amplitude) these singularities and discontinuities are smoothed out over a radial distance of order $\gamma/|\omega_e'(r_{beat})|$. In other words, for finite pump amplitude A_p the unstable eigenmode becomes a discrete eigenmode in the eigenvalue problem given by Eqs. (56) and (57).

An example of the vorticity perturbation for finite pump amplitude is displayed in Fig. 7 for $3 \to 2$ decay, calculated by solution of the matrix eigenvalue problem obtained by discretizing radial position in Eqs. (56) and (57). For a radial grid with M elements ($M = 2000$ in the figure), there are $M+1$ eigenmodes in this problem. $M-2$ of the modes are discretized versions of singular continuum modes analogous to the continuum modes of the unforced Kelvin/diocotron problem, discussed previously in relation to Eq. (20) and displayed in Fig. 3. The other three eigenmodes are discrete (i.e., with continuous eigenfunctions). One of these discrete modes is the $l = l_b$ Kelvin/diocotron mode. The other two discrete eigenmodes have complex frequencies and eigenfunctions that are conjugate to one-another, so one

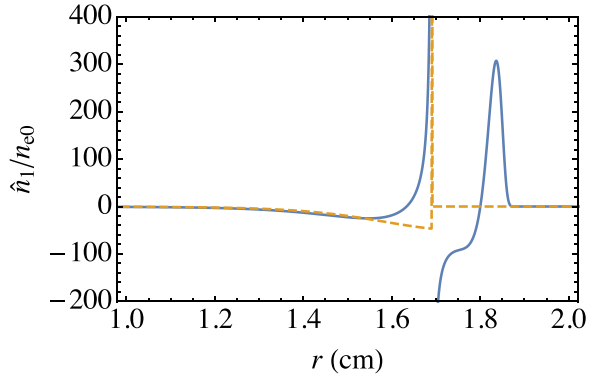

FIG. 6. Real (solid) and imaginary (dashed) components of the scaled radial dependence $\hat{n}_{l_b}(r)$ of the beat wave vorticity perturbation $n_{l_b}(r,t) = A_pA_{di}^*e^{-i\bar{\omega}t}\hat{n}_{l_b}(r)$ for the $3 \to 2$ decay, corresponding to the beat wave stream function $\hat{\phi}_{l_b}(r)$ in Fig. 5. The imaginary part of $\hat{n}_{l_b}$ is proportional to a single continuum eigenfunction $n_{l_b,\alpha}(r)$ [a solution of Eq. (20)], with α determined by the beat wave resonance condition $\omega_{l_b,\alpha} = \Delta\omega$.

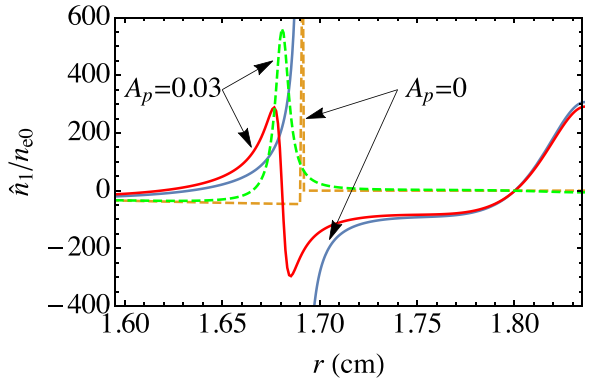

FIG. 7. Real (solid) and imaginary (dashed) components of the radial dependence $\hat{n}_{l_b}(r)$ of the beat wave vorticity perturbation $n_{l_b}(r,t) = A_pA_{di}^*e^{-i\bar{\omega}t}\hat{n}_{l_b}(r)$ for $3 \to 2$ decay and for two dimensionless pump amplitudes: $A_p = 0.03$ and $A_p \to 0$ (the latter limit is the same as in Fig. 6; note the change in scale of the x and y axes). At finite pump amplitude, the beat wave vorticity perturbation is no longer singular; it is the l_b Fourier component of a discrete unstable eigenmode, a solution of Eqs. (56) and (57).

grows in time and the other decays. The real and imaginary parts of the eigenmode corresponding to exponential growth are plotted in Fig. 7 and is compared to the infinitesimal amplitude case plotted in Fig. 6. Note that the vector eigenmode $(A_{di}^*, \tilde{n}_{l_b}(r))$ can have an arbitrary overall amplitude, but the ratio $\tilde{n}_{l_b}(r)/A_{di}^*$ is uniquely determined, and this is what is plotted in the figure, scaled by A_p as well in order to produce $\hat{n}_{l_b}$ [see Eq. (74)] and to compare to Fig. 6.

In addition to resonance broadening at finite pump amplitude, there is a small but noticeable decrease in the radius of the resonance. This is explained by the nonlinear increase $\delta\omega$ in the real frequency of the eigenmode as shown in Table I. This frequency increase shifts the position of the Landau resonance to smaller radius according to $l_b\omega_e(r) = \Delta\omega + \delta\omega$.

In Table I, we display the theoretically predicted growth rates in beat wave decay, for a range of Kelvin/diocotron mode numbers. For $l_p = 2, l_d = 1$, the growth rate is zero. This is an analytic result based on Eq. (80), using Eq. (81) for the imaginary part of the scaled radial derivative of the beat wave stream function, $\hat{\phi}_i'(r_w)$. Since this function is zero at all radii beyond the resonant radius r_{beat}, the growth rate vanishes. The rate is also small and decreasing with increasing l_p for $l_p > 2, l_d = 1$. In these decays, the wall is far enough from the vortex that there is almost no coupling of the pump wave to the $l_d = 1$ mode.

In general, growth rates increase with increasing daughter wave mode number l_d. The experiments also observe this trend as shown by the final column in the table, with measured growth rates of similar size to those evaluated theoretically. This column will be discussed in more detail in Sec. IV.

2. Other nonlinear effects on Kelvin/diocotron waves: Frequency shifts and the Love instability

Frequency shifts caused by the pump wave in typical experimental conditions are small, of order $A_p^2 \ll 1$, but might still be observed in the experiments, so it is worthwhile to pursue them theoretically. We start with the frequency shift $\delta\omega_p$ to the pump wave itself. We

TABLE I. Frequency shifts and growth rates in beat wave decay for the experimental density profile of Fig. 2.

Decay process	Unperturbed pump frequency	Unperturbed daughter frequency	Frequency shift contribution	Growth rate	Experimental growth rates
l_p, l_d, l_b	$\frac{\omega_{l_p,K}}{\omega_{e0}}$	$\frac{\omega_{l_d,K}}{\omega_{e0}}$	$\frac{\delta\omega}{\omega_{e0}A_p^2}$	$\frac{\gamma}{\omega_{e0}A_p^2}$	$\frac{\gamma_{\exp}}{\omega_{e0}A_p^2}$
5 4 1	3.72	2.83	64.3	27.9	20.6 (Fig. 16)
5 3 2		1.92	21.0	10.9	10.
5 2 3		1.02	6.07	2.00	3.1
5 1 4		0.22	-9.6×10^{-6}	4.1×10^{-7}	0
4 3 1	2.83	1.92	20.7	11.1	7.86 (Fig. 15)
4 2 2		1.02	6.43	2.29	2.1
4 1 3		0.22	-1.2×10^{-4}	2.4×10^{-6}	0
3 2 1	1.92	1.02	6.78	2.77	2.73 (Fig. 14)
3 1 2		0.22	−0.0015	8.0×10^{-6}	0
2 1 1	1.02	0.22	−0.017	0	0

have not considered this shift so far. For an $l_p = 2$ mode on an isolated vortex patch, the nonlinear mode frequency was determined by Kirchhoff for arbitrary amplitudes.[32] For general mode numbers, the frequency shift was evaluated by Burbea, also for an isolated vortex patch, using an elegant conformal mapping method.[33] Burbea obtained, to lowest order in A_p,

$$\delta\omega_p = -A_p^2 n_e l_p (l_p - 1). \tag{90}$$

This formula is generalizable to the case where the patch is contained within walls of finite radius r_w,

$$\delta\omega_p = -A_p^2 n_e l_p \frac{1 - 2\rho^{2l_p}}{(1-\rho^{2l_p})^2}\left[(l_p-1)(1-2\rho^{2l_p}) - (1+l_p)\rho^{4l_p}\right], \tag{91}$$

where $\rho \equiv r_p/r_w$. For $l_p = 1$, this expression agrees with the nonlinear frequency shift of an $l_p = 1$ mode derived by Fine.[34] Equation (91) also reduces to Eq. (90) in the $\rho \to 0$ limit. The formula follows from a perturbation analysis of the vortex patch edge. The edge is deformed by the mode to

$$R(\theta, t) = r_p \frac{1 + 2A_p \cos(l_p\theta - \omega_p t) + A_p^2 B \cos 2(l_p\theta - \omega_p t) + \cdots}{\sqrt{1 + 2A_p^2 + A_p^4 B^2/2 + \cdots}} \tag{92}$$

[a nonlinear generalization of Eq. (16)], where $A_p^2 B$ is the amplitude of the second harmonic, and the denominator is chosen so that the area enclosed by the contour is πr_p^2, independent of mode amplitude A_p. This is required by the incompressible nature of the flow. The value of B and the nonlinear pump wave frequency $\omega_p = \omega_{l_p,K} + \delta\omega_p$ can then be found by satisfying the dynamical equation for the edge of the vortex,[35]

$$\frac{\partial R}{\partial t} + \frac{v_\theta(\theta, t)}{R}\frac{\partial R}{\partial \theta} = v_r(\theta, t), \tag{93}$$

where $v_\theta = -\partial\phi/\partial r|_{r=R}$ and $v_r = \partial\phi/\partial\theta|_{r=R}$ are the θ and r components, respectively, of the fluid velocity evaluated at the vortex edge, and ϕ is the stream function of the deformed vortex patch. The dynamical equation is then solved in a power series expansion in A_p order by order. Incidentally, this expansion can be automated by using computer algebra manipulation, to produce analytic expressions for the frequency shift and the shape of the patch to arbitrary order in A_p. The results reproduce the numerically determined large amplitude mode results of Deem and Zabusky.[36]

At large amplitudes, an instability in the nonlinear mode is predicted to occur, termed the Love instability, after A. E. H. Love, who analyzed the instability of large amplitude $l_p = 2$ Kelvin modes on an isolated vortex patch.[24] The Love instability occurs when one of the eigenmodes of the deformed vortex patch approaches zero frequency (as seen in the frame of the pump wave), and causes a bifurcation of the deformed equilibrium to a new equilibrium containing both higher and lower azimuthal mode numbers. The instability has been observed for $l_p = 2$ in nonneutral plasma experiments[37] and contour dynamics simulations.[38]

For larger values of l_p, the Love instability has been studied analytically and numerically on uniform vortex patches.[39] This instability is quite different from the beat wave decay instability. There is an amplitude threshold for onset of the Love instability, and also, the excited waves have substantial contributions from both higher and lower mode numbers, unlike the decay instability where the energy is transferred mainly to lower mode numbers, and where growth rates are finite for all finite pump amplitudes. Finally, the Love instability can occur for a vortex patch, but beat wave decay cannot, as it requires a finite vorticity gradient at the resonant radius r_{beat} within the vortex.

Returning to the question of frequency shifts, for a general nonuniform vortex with an edge of finite width, the frequency shift of the pump wave caused by finite pump amplitude has not been considered theoretically to our knowledge, although the shift has been observed in recent experiments.[15] The frequency shift to the l_d daughter wave caused by the finite pump amplitude has also not been considered. We determined one portion of the shift to the daughter wave frequency, $\delta\omega$, in Sec. III A 1, caused by mode coupling to the l_b beat wave. However, there are two other shifts that have not yet been considered. First, the pump wave changes the $l = 0$ component of the vorticity at second order in A_p^2, which in effect changes the equilibrium vorticity

used to determine the mode frequency. This effect is purely geometrical, producing a frequency shift $\delta\omega^{(1)}$ due to the shift in the contours of constant vorticity caused by the pump wave. Second, nonlinear coupling of the daughter wave to the pump wave produces a second beat wave at wavenumber $l_p + l_d$, which then couples back to l_d to produce a frequency shift $\delta\omega^{(2)}$. If we take $l_d = l_p$ then this same calculation provides the pump wave shift. Each of these two effects can be considered separately, producing frequency shifts $\delta\omega^{(1)}$ and $\delta\omega^{(2)}$ that can be added to obtain the total nonlinear shift in the frequency to either the pump wave or the daughter wave.

We first consider the $0(A_p^2)$ change to the $l=0$ vorticity profile caused by the pump wave. On a nonuniform vortex, a given contour of constant vorticity deforms from a circle of radius r to a curve with radial variation in θ which, in the rotating frame of the mode, is a generalization of Eq. (92),

$$R(\theta, r) = r\frac{r + 2A_p r_{l_p}(r)\cos l_p\theta + A_p^2 B(r)\cos 2l_p\theta + \cdots}{\sqrt{r^2 + 2A_p^2 r_{l_p}(r)^2 + A_p^4 B(r)^2/2 + \cdots}}, \quad (94)$$

where $r_{l_p}(r) = -n_{l,K}(r)/n_e'(r)$ is the radial displacement caused by the pump wave in linear theory, and $B(r)$ is the nonlinear correction, now a function of radius. The denominator is again determined by the incompressibility of the flow, so that the area enclosed by the contour is πr^2. Now, the vorticity $n(r,\theta)$ in the presence of the pump wave is expressed as

$$n(R,\theta) = n_e(r(R,\theta)), \quad (95)$$

where $r(R,\theta)$ is the function obtained by taking the inverse of Eq. (94). This follows from the fact that the solution of the continuity equation (1) is that vorticity is constant along the equation's characteristics.

This equation can be evaluated as a power series in A_p and to second order yields

$$\begin{aligned} n(R,\theta) = {} & n_e(R) - 2A_p r_{l_p}(R) n_e'(R)\cos l_p\theta \\ & + A_p^2\left[n_e'(R)\left(\frac{r_{l_p}^2(R)}{R} + 2r_{l_p}(R)r_{l_p}{}'(R)\right) + n_e''(R)r_{l_p}^2(R)\right] \\ & + A_p^2\cos(2l_p\theta)\Big[n_e'(R)(-B(R) \\ & + 2r_{l_p}(R)r_{l_p}{}'(R)) + n_e''(R)r_{l_p}^2(R)\Big]. \end{aligned} \quad (96)$$

The $l=0$ vorticity component is the θ average, $n_0(r) = \int d\theta n(r,\theta)/(2\pi) = n_e(r) + \delta n_0(r)$ with the change $\delta n_0(r)$ given by

$$\delta n_0(r) = A_p^2\left[n_e'(r)\left(\frac{r_{l_p}^2(r)}{r} + 2r_{l_p}(r)r_{l_p}{}'(r)\right) + n_e''(r)r_{l_p}^2(r)\right]. \quad (97)$$

Using an integration by parts one can easily show that the change in total circulation, $\int d^2r\delta n_0$, is identically zero, as one would expect.

However, this vorticity perturbation does cause a variation $\delta\omega_e(r)$ in the $E\times B$ rotation rate of the vortex,

$$\delta\omega_e(r) = A_p^2\frac{r_{l_p}^2(r)}{r}n_e'(r). \quad (98)$$

Adding these terms to mode equation (20) for a Kelvin/diocotron wave of mode number l_d, the equation becomes

$$\omega n_{l_d} = \hat{L}n_{l_d} + l_d\delta\omega_e n_{l_d} + \frac{l_d}{r}\delta n_0'\phi_{l_d}. \quad (99)$$

Taking an inner product with respect to eigenmode vorticity $n_{l_d,K}$ then yields the lowest order frequency shift,

$$\delta\omega^{(1)} = \omega - \omega_{l_d,K} = l_d\frac{\left\langle n_{l_d,K}, \delta\omega_e n_{l_d,K} + \frac{1}{r}\delta n_0'\phi_{l_d,K}\right\rangle_P}{P_{l_d,K}}, \quad (100)$$

where $P_{l_d,K} = \langle n_{l_d,K}, n_{l_d,K}\rangle_P$ is the scaled angular momentum of the diocotron eigenmode.

For $l_d = 1$, an evaluation of the inner product shows that this frequency shift vanishes, as expected, since a change to the equilibrium radial vorticity profile has no effect on the $l_d = 1$ mode frequency provided that total circulation Γ is conserved, see Eq. (18).

Incidentally, the eigenmode angular momentum $P_{l_p,K}$ can be directly evaluated from the $l=0$ vorticity perturbation δn_0 using the definition of angular momentum, Eq. (10),

$$\begin{aligned} \frac{\delta\mathscr{P}}{\rho_0 A_p^2} &= -\frac{1}{2A_p^2}\int d^2r r^2\delta n_0(r) \\ &= -\frac{1}{2}\int 2\pi r dr r^2\left[n_e'(r)\left(\frac{r_{l_p}^2(r)}{r} + 2r_{l_p}(r)r_{l_p}{}'(r)\right) + n_e''(r)r_{l_p}^2(r)\right] \\ &= \int 2\pi dr r^2 n_e'(r)r_{l_p}^2(r) = 2P_{l_p,K}, \end{aligned} \quad (101)$$

where in the last line an integration by parts on the $n_e''(r)$ term was applied. This calculation verifies the functional form of eigenmode angular momentum given in Eqs. (30) and (29). The change in angular momentum is twice the eigenmode angular momentum $P_{l_p,K}$ because $\pm l_p$ eigenmodes contribute equally to the vorticity perturbation.

Turning now to the frequency shift $\delta\omega^{(2)}$ due to mode coupling of l_d and l_p, we first evaluate the nonlinear mode equation (7) for the second beat wave at mode number $l_p + l_d \equiv l_{b_2}$, with frequency $\omega_{l_p,K} + \omega_{l_d,K} \equiv \omega_{b_2}$. To do so we use Eq. (44) for the pump wave, and the linear form for the daughter wave vorticity perturbation,

$$\tilde{n}_{l_d}(r) = A_d n_{l_d,K}(r). \quad (102)$$

The equation for the l_{b_2} vorticity harmonic is then

$$(\omega_{b_2} - l_{b_2}\omega_e(r))\tilde{n}_{l_{b_2}} = \frac{l_{b_2}}{r}n_e'(r)\tilde{\phi}_{l_{b_2}} + A_pA_dF_{b_2}(r), \quad (103)$$

where the mode coupling term F_{b_2} is

$$\begin{aligned} F_{b_2}(r) = {} & \frac{l_d}{r}(\phi_{l_d,K}n_{l_p,K}' - n_{l_d,K}\phi_{l_p,K}') \\ & + \frac{l_p}{r}(\phi_{l_p,K}n_{l_d,K}' - n_{l_p,K}\phi_{l_d,K}') \quad \text{if } l_d \neq l_p, \end{aligned} \quad (104)$$

$$F_{b_2}(r) = \frac{l_p}{r}(\phi_{l_p,K}n_{l_p,K}' - n_{l_p,K}\phi_{l_p,K}') \quad \text{if } l_d = l_p. \quad (105)$$

Solving Eq. (103) for $\tilde{n}_{l_{b_2}}$ in terms of $\tilde{\phi}_{l_{b_2}}$ and the driving term F_{b_2}, we substitute for $\tilde{n}_{l_{b_2}}$ into the Poisson equation (8) and solve the resulting inhomogeneous boundary value problem for $\tilde{\phi}_{l_{b_2}}$, providing the beat wave vorticity and stream function. Since the driving term is proportional to A_pA_d, the beat wave is also proportional to these amplitudes, so we write

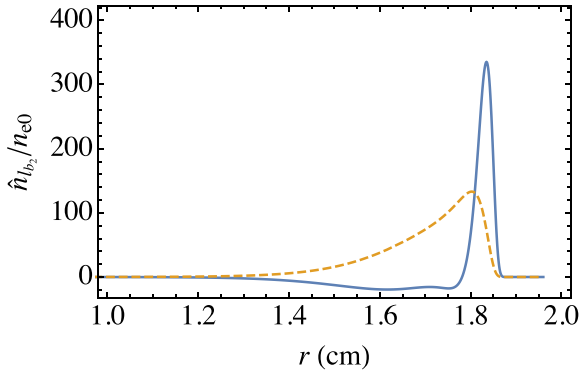

FIG. 8. Solid curve: scaled vorticity $\hat{n}_{l_{b_2}}$ of the second beat wave, at mode number $l_{b_2} = l_p + l_d$ for the case $l_p = 3, l_d = 2$. Dashed curve: the $l = 5$ Kelvin/diocotron wave component of the beat wave vorticity.

$$\tilde{n}_{l_{b_2}} = \hat{n}_{l_{b_2}} A_p A_d, \quad \tilde{\phi}_{l_{b_2}} = \hat{\phi}_{l_{b_2}} A_p A_d, \tag{106}$$

where $\hat{n}_{l_{b_2}}$ and $\hat{\phi}_{l_{b_2}}$ are scaled so as to be independent of the pump and daughter amplitudes. An example solution for the scaled vorticity $\hat{n}_{l_{b_2}}$ is shown in Fig. 8 for the case $l_d = 2, l_p = 3$. The contribution to this $l_{b_2} = 5$ beat wave of the $l = 5$ Kelvin/diocotron mode is displayed as the dashed line. One can see that much of the beat wave perturbation is due not to the discrete mode but due to $l_{b_2} = 5$ continuum modes. However, unlike the main beat wave with mode number l_b, there is no Landau resonance with $\omega_{b_2} = l_{b_2}\omega_e$ within the vortex, so there is no resonant response and no contribution to the growth rate, only a frequency shift.

The frequency shift $\delta\omega^{(2)}$ can now be evaluated by accounting for the l_{b_2} mode in the l_d nonlinear mode equation (7),

$$\omega n_{l_d} = \hat{L} n_{l_d} + A_p^2 A_d \bar{F}_d(r), \tag{107}$$

where

$$\bar{F}_d(r) = \frac{l_{b_2}}{r}(\hat{\phi}_{l_{b_2}} n'_{l_p,K} - \hat{n}_{l_{b_2}} \phi'_{l_p,K}) - \frac{l_p}{r}(\phi_{l_p,K} \hat{n}'_{l_{b_2}} - n_{l_p,K} \hat{\phi}'_{l_{b_2}}). \tag{108}$$

Substituting for n_{l_d} using Eq. (102) and taking an inner product with respect to $n_{l_d,K}$ then yields the frequency shift,

$$\delta\omega^{(2)} = \omega - \omega_{l_d,K} = A_p^2 \frac{\langle n_{l_d,K}, \bar{F}_d \rangle_p}{P_{l_d,K}}. \tag{109}$$

The total shift is then the sum of $\delta\omega^{(1)}$ and $\delta\omega^{(2)}$. For $l_d = l_p$, the result is the pump wave frequency shift, $\delta\omega_p = \delta\omega^{(1)} + \delta\omega^{(2)}$.

We have performed this evaluation for a few of the modes, for the vorticity profile shown in Fig. 2. The resulting pump wave frequency shifts are given in Table II and compared to expression (91) for a uniform vortex patch. For smaller mode numbers, the formula for the experimental profile, the sum of Eqs. (100) and (109), provides a frequency shift that is fairly close to that for a uniform patch, Eq. (91), with similar ratio of plasma to wall radius chosen as $\rho = 1/2$. For $l_p > 3$, however, the pump wave frequency shift for a nonuniform profile increases rapidly compared to that for a patch. This is because the resonant radius $r_{l_p,K}$ becomes closer to the edge of the plasma (see Fig. 2). Integrals required in Eqs. (100) and (109) exhibit divergences and $\delta\omega_p$ diverges to negative infinity as $r_{l_p,K}$ approaches the region of finite vorticity. Physically, only very small mode amplitudes are required to push the vorticity to a radius where it becomes resonant with the mode, forming a cat's eye that cannot be described using perturbation theory. In this situation, a perturbation theory for a nonlinear mode is relevant only for very small amplitudes, before cat's eyes become important. To describe larger amplitudes it would be useful to construct "BGK"-like stationary states[40] that include the vorticity trapped in the cat's eyes. We leave this more sophisticated analysis to future work.

TABLE II. Nonlinear frequency shifts of Kelvin/diocotron pump and daughter waves.

Pump mode l_p	Daughter mode l_d	Pump frequency shift using exp. profile $\frac{\delta\omega_p}{\omega_{e0}A_p^2}$	Pump frequency shift for patch, Eq. (91) $\frac{\delta\omega_p}{\omega_{e0}A_p^2}\Big\vert_{\rho=1/2}$	Daughter frequency shift $\frac{\delta\omega_d}{\omega_{e0}A_p^2}$
1	1	0.180	0.222	
2	2	−3.44	−3.44	
2	1			0.15
3	3	−12.8	−11.6	
3	2			−6.00
3	1			0.043
4	4	−36.3	−23.8	
4	3			−16.2
4	2			−6.28
4	1			0.012
5	5	−117.3	−39.9	
5	4			−44.2
5	3			−21.5
5	2			−6.81
5	1			0.0034

However, some idea of the effect of particle trapping in cat's eyes can be obtained through particle in cell simulations, which we have performed for a range of mode amplitudes. The simulations follow 8×10^6 particles with time advanced using a third-order accurate Adams Bashforth method. To evaluate the velocity field at each time step, the Poisson equation for the stream function $\phi(x, y, t)$ is solved on a uniform square grid with grid spacing $\Delta x = \Delta y = r_w/201$, keeping grid points within a circular boundary at $r = r_w$, and with boundary condition $\phi = 0$ at $r = r_w$ evaluated by linear interpolation between boundary grid points just inside and outside the circular domain.[41] The Poisson equation on this grid is reduced to a linear matrix problem by standard second-order discretization of the Laplacian operator, and solved using the Slatec routine SNBFS. Particles are arranged initially to produce the experimental equilibrium vorticity profile of Fig. 2, and with an approximation to an $l_p = 4$ Kelvin/diocotron mode of amplitude A_p added to the initial condition, $n(r, t = 0) = n_e(r/(R(\theta, 0)/r_p))$, with $R(\theta, 0)$ given by Eq. (92).

Oscillations in moments of the vorticity can then be observed, whose frequencies are similar to those expected in perturbation theory for a vortex patch, Eq. (91), provided that the mode amplitude is

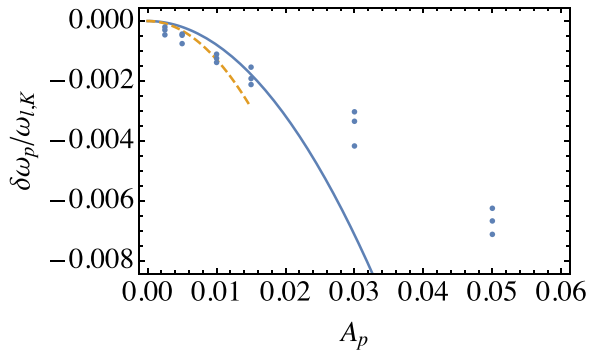

FIG. 9. Nonlinear shift $\delta\omega_p = \omega_p - \omega_{l_p,K}$ in the Kelvin/diocotron mode frequency vs pump amplitude A_p compared to the theoretical linear frequency $\omega_{l_p,K}$, for an $l_p = 4$ mode on a vortex with the equilibrium profile of Fig. 2. Solid curve is the theory for a vortex patch, Eq. (91), where $\omega_{l_p,K}$ is given for a patch by Eq. (15). Dashed curve is the shift given in Table II for the nonuniform vorticity profile used in the simulation, with $\omega_{l_p,K}$ determined by the shooting method. Dots give values of $\delta\omega_p$ obtained in particle in cell simulations, with $\omega_{l_p,K}$ again given by the shooting method.

sufficiently small; see Fig. 9. Note that the downward shift appears somewhat larger than expected from the patch theory, and might be argued to agree better with the theory for a nonuniform patch in this small amplitude regime, but scatter in the data makes the size of the discrepancy difficult to interpret. An example of the particle positions at the end of a run is shown in Fig. 10 for an $l_p = 4$ mode with small amplitude, $A_p = 0.005$; there are no significant cat's eyes at this amplitude. However, for somewhat larger amplitudes, trapping in cat's eyes starts to occur (Fig. 11). The mode frequencies then begin to deviate significantly from the relatively large downward shift expected in perturbation theory (Fig. 9).

We have also determined the frequency shift contributions to the l_d daughter wave, $\delta\omega^{(1)} + \delta\omega^{(2)}$, when $l_d < l_p$. The total frequency shift to the l_d mode is then $-\delta\omega + \delta\omega^{(1)} + \delta\omega^{(2)} \equiv \delta\omega_d$. (Recall that the shift $\delta\omega$ is to the $-l_d$ mode frequency, while we define $\delta\omega_d$ as the

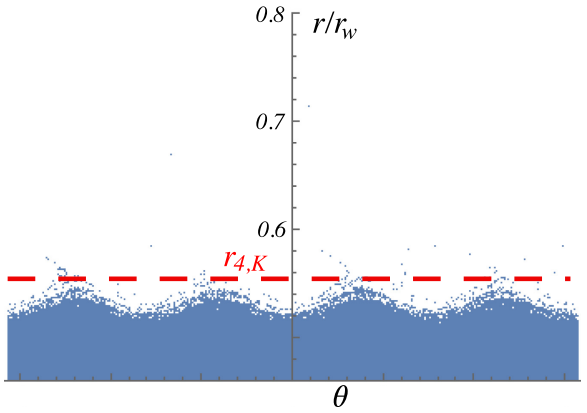

FIG. 10. Particle positions in the edge of a vortex after 25 oscillation periods in a particle in cell simulation of a small amplitude ($A_p = 0.005$) $l_p = 4$ Kelvin/diocotron mode on a vortex with the equilibrium vorticity profile of Fig. 2. The resonant radius $r_{4,K}$ is shown as the dashed line.

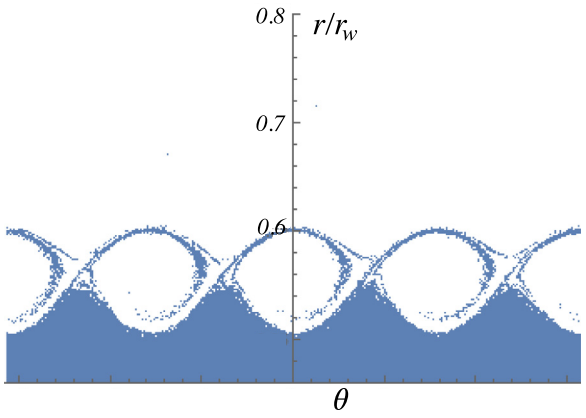

FIG. 11. Particle positions in a larger amplitude $l_p = 4$ mode after 25 periods, with $A_p = 0.015$.

shift to the $+l_d$ mode; this explains the minus sign in the equation for $\delta\omega_d$.) In Table II, we tabulate $\delta\omega_d$ values for all relevant values of l_p and l_d, for the experimental density profile of Fig. 2.

To summarize, when frequency shifts are included up to $0(A_p^2)$ in the pump wave amplitude, the pump wave frequency is $\omega_p = \omega_{l_p,K} + \delta\omega_p$, the l_d daughter wave frequency is $\omega_d = \omega_{l_d,d} + \delta\omega_d$, and the beat wave has frequency $\omega_b = \omega_p - \omega_d = \omega_{l_p,K} - \omega_{l_d,K} + \delta\omega_p - \delta\omega_d$.

IV. EXPERIMENTS ON BEAT WAVE DECAY

We have performed a series of experiments to observe beat wave decay. The experiments employ a pure electron plasma trapped in a cylindrical Penning trap. The trap consists of a set of hollow cylindrical electrodes of radius $r_w = 3.5$ cm, with the end electrodes biased negatively to -100 V in order to provide a potential well that traps electrons in the axial (z) direction (Fig. 12). In these experiments the plasma length is roughly 34 cm. Radial trapping is provided by an applied magnetic field $B\hat{z}$, with a strength of $B = 12$kG. In order to measure the z–integrated plasma density, the plasma can be dumped onto a phosphor screen by lowering the end confinement potential, and the emitted light from the phosphor is then captured by a CCD camera. Dividing the z-integrated density by the plasma length then provides the plasma number density $N^{expt}(r, \theta, t)$. A typical equilibrium radial density profile $N_e^{expt}(r)$ is displayed in Fig. 2, normalized to the central density. With the exception of a small tail at large radius,

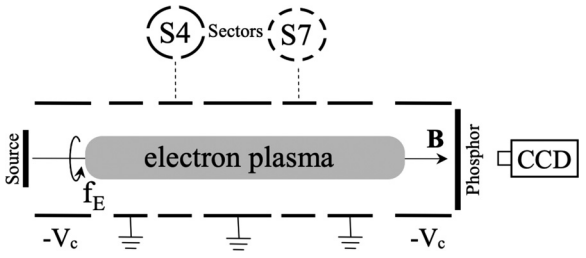

FIG. 12. Schematic of the experimental apparatus.

which we neglect in the theory, this density can be fit by a fairly simple functional form that is used in the theory of Secs. II and III,

$$N_e(r) = N_{e0} \exp\left\{-b\left[(1 + e(r/r_c)^{50})(r/r_p)\right]^f\right\}(1 - c(r/r_p)^2), \tag{110}$$

where $b = 32.2, c = 0.036, f = 13.6$, the approximate plasma radius is $r_p = 2.2$cm, the cut off radius is $r_c = 1.95$cm, the central density is $N_{e0} = 9.88 \times 10^6 \text{cm}^3$, and $e = 1$. A smooth form for the density, rather than noisy experimental data, is required in the theory because derivatives of the density are needed. The listed N_{e0} value is obtained from comparison of measured diocotron mode frequencies to theory for the given density profile, which gives a more accurate value of the central density than the phosphor screen can provide. We should also note that there is shot to shot variation in the overall particle number of order 1%, and shot to shot variation in the plasma radius by about 1% as well. Also, the value $e = 0$ gives a better fit to the density data shown in Fig. 2 in the edge region of the plasma, but the value $e = 1$ is chosen instead in order to smoothly eliminate a small portion of the edge density beyond the listed cutoff radius r_c, so as to remove weak Landau resonances for the $l = 4$ and $l = 5$ pump modes, allowing a description of these modes as discrete linear eigenmodes. We completely neglect the low-density tail observed in the experimental data (Fig. 2) at larger radii, for the same reason. For $l \leq 3$, either value of e can be taken without much change to theory results ($< 1\%$ on eigenmode frequencies, $< 10\%$ on growth rates and frequency shifts), except for the functional form of the $l = 2$ and $l = 3$ diocotron mode density perturbations, which are more accurately described by the $e = 0$ theory.

Diocotron modes are excited on the plasma column by applying oscillating voltages to the sectored electrode labeled S7 in Fig. 12, which consists of eight 25° sectors. We apply 15–30 cycles of properly phase-shifted oscillating voltages (with amplitude up to several volts) to two adjacent sectors to excite the pump mode of interest. Frequency selection implies that simultaneous excitation of other diocotron modes is at least two orders of magnitude smaller in amplitude. A third sector on S7 is used to detect image current in order to monitor the frequency and amplitude of the resulting diocotron wave(s) as a function of time. An example is displayed in Fig. 13. Here, $t = 0$ corresponds to the time directly after the oscillating voltage is turned off, 10 s after initial injection of the plasma into the Penning-Malmberg trap. This 10 s period is used to prepare the equilibrium density profile. In this example an $l_p = 3$ pump wave is excited with amplitude $A_p(t)$, and an $l_d = 2$ daughter diocotron mode with amplitude $A_d(t)$ subsequently grows out of noise, with a measured growth rate in this case of $\gamma^{expt} = 13.6 \text{s}^{-1}$. No $l_b = 1$ beat wave signal is observed in the experiment, presumably because the signal is below the noise floor of the measurements. [Recall that the beat wave wall signal is expected to be small, as discussed in relation to Eq. (89).] However, as discussed later, the $l_b = 1$ beat wave density perturbation can be observed using the phosphor screen dump diagnostic.

This experiment is then repeated for a range of initial pump amplitudes A_p. The resulting growth rates are plotted vs amplitude in Fig. 14. The theory for the rate for the best-fit equilibrium profile of Eq. (110), given in Table I, is $\gamma = 2.77 A_p^2 \omega_{e0}$, which is within two percent of the value obtained from a fit to the growth rate data, $\gamma^{fit} = 2.73 A_p^2 \omega_{e0}$.

This process was repeated for $4 \to 3$ and $5 \to 4$ decays, and the resulting growth rates are plotted vs pump amplitude in Figs. 15 and 16. The theory for the growth rates is given in Table I, $\gamma^{4\to3} = 11.1 A_p^2 \omega_{e0}$, and $\gamma^{5\to4} = 27.9 A_p^2 \omega_{e0}$. For both decays, the predicted growth rate is somewhat larger than the experimental fits, $\gamma^{fit} = 7.86 A_p^2 \omega_{e0}$ for the $4 \to 3$ case and $\gamma^{fit} = (-4.6 \times 10^{-4} + 20.6 A_p^2)\omega_{e0}$ for the $5 \to 4$ decay. For the $5 \to 4$ decay, a slight negative offset, $-4.6 \times 10^{-4} \omega_{e0}$ is added to the fit to better match the growth rate data. It is likely that this offset is caused by linear Landau damping of the $l_d = 4$ daughter wave.

Other decays have also been observed and measured growth rates are compared to theory in Table I, for several of these decay processes. For the case of $3 \to 2$, $4 \to 3$, and $5 \to 4$ decays, the quoted value in the Table is γ^{fit} from the data in Figs. 14–16. For other cases, the quoted values are from single evolutions similar to that shown in Fig. 13. These growth rates also follow the general trend of the theory that rates are increasing functions of the daughter wave mode number l_d.

For $l_b = l_d = 1$ (i.e., a $2 \to 1$ decay), the theory value of γ is $\gamma = 0$. This follows analytically from Eq. (80) along with the fact that $\Im\hat{\phi}_{l_b}(r) = 0$ for $r > r_{beat}$; see Eq. (81). The measured value for $2 \to 1$

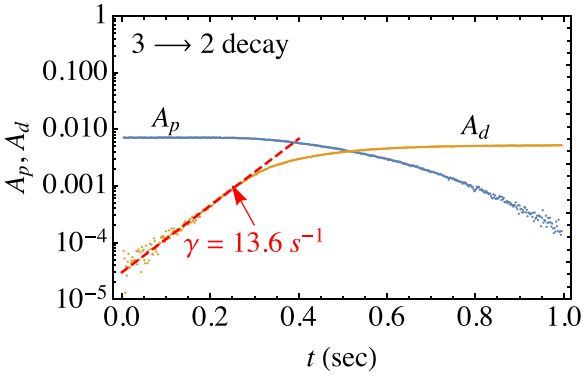

FIG. 13. Amplitude vs time for an $l_p = 3$ pump wave (labeled A_p) and an $l_d = 2$ daughter wave (labeled A_d), measured from the signals induced on sectored cylindrical electrodes, and an exponential fit to the daughter wave amplitude.

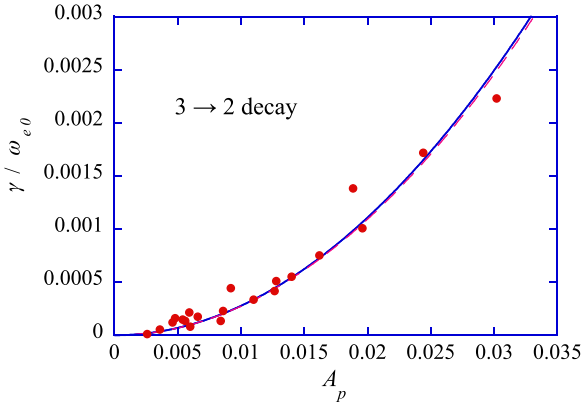

FIG. 14. Experimental decay rates for $3 \to 2$ decay, normalized by the central rotation rate $\omega_{e0} = 74.5$krad/s, vs pump amplitude A_p. Solid curve is the theory for the rate, and the dashed curve is a quadratic fit to the data.

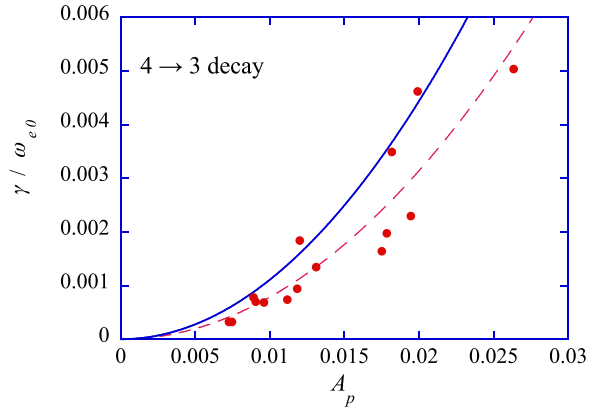

FIG. 15. Experimental decay rates for 4 → 3 decay, normalized by the central rotation rate $\omega_{e0} = 74.5\text{krad/s}$, vs pump amplitude A_p. Solid curve is the theory for the rate, and the dashed curve is a quadratic fit to the data.

decay is also zero, consistent with the theory, to within experimental accuracy. In more detail, there is an observed (very) small growth of the $l_d = 1$ diocotron mode that we have determined to be caused by the resistive wall instability,[42] with a growth rate of 0.0037s^{-1}. This growth rate can be varied by adding or removing resistors between the sectored electrodes. However, keeping such resistances as small as possible, this $l_d = 1$ growth rate is independent of whether or not an $l_p = 2$ pump wave is launched, and therefore, to experimental accuracy we measure a beat wave growth rate of zero.

Similarly, for all $l_d = 1$ decays with $l_p > 2$, both γ and $\delta\omega$ are predicted to be nonzero but extremely small, according to Eq. (80) and the numerical solution for $\hat{\phi}_{l_p}$ discussed previously; see Table I. These decays were also not observed in the experiments; i.e., the small resistive growth rate of the $l_d = 1$ mode was unaffected by the launch of any pump wave.

In addition to the measured growth rates, the dump diagnostic can provide an instantaneous measurement of density perturbations in the plasma. In Fig. 17, we display the density $N(r, \theta)$ obtained from a

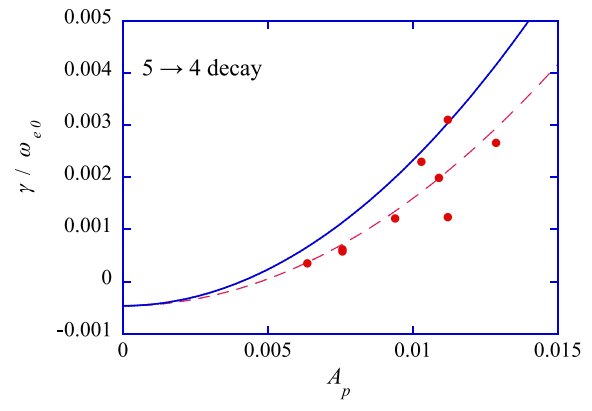

FIG. 16. Experimental decay rates for 5 → 4 decay, normalized by the central rotation rate $\omega_{e0} = 74.5\text{krad/s}$, vs pump amplitude A_p. Solid curve is the theory for the rate, shifted to account for weak linear mode damping, and the dashed curve is a quadratic fit to the data.

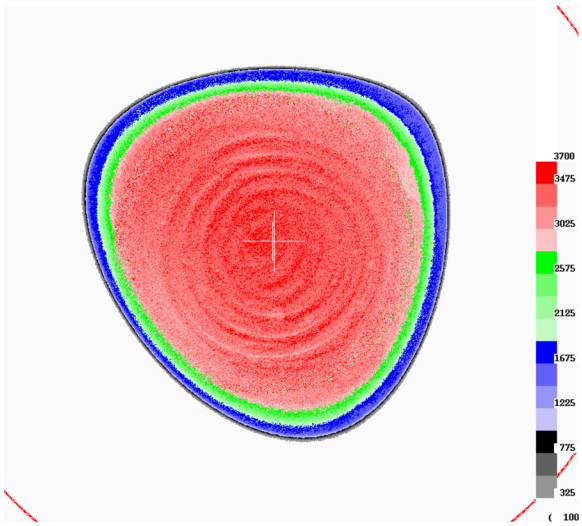

FIG. 17. Color contour map of plasma density $N(r, \theta)$ measured via the dump diagnostic at the end of a 3 → 2 decay experiment. The linear color scale on the right is in arbitrary units. The red arcs at the edge of the image indicate the wall radius, $r_w = 3.5\,\text{cm}$, and the cross at the center indicates the geometrical center of the trap electrodes. The faint spiral in the central region is an artifact caused by a burn in the phosphor.

CCD image of the phosphor screen after a plasma dump at the end of a 3 → 2 decay experiment. One can observe an obvious $l = 3$ perturbation in the image, along with a less obvious $l = 2$ perturbation. By Fourier analyzing the data in θ, we can then obtain $n_l(r)$ for different mode numbers l, and the magnitude of these Fourier components are shown in Figs. 18–20. The dimensionless amplitudes A_l can also be computed directly from $N(r, \theta)$ using Eq. (19). The magnitudes are, for $l = 3$, $|A_p| = 0.03$ and for $l = 2$, $|A_d| = 0.02$. This is a comparatively large amplitude pump wave, and the daughter wave has grown until it is almost as large. The dashed lines in Figs. 18 and 19 are the theory predictions for the Kelvin/diocotron eigenfunctions at the given amplitudes, which are reasonably good fits to the experimental data [for these plots we have taken $e = 0$ in Eq. (110); the fit would be

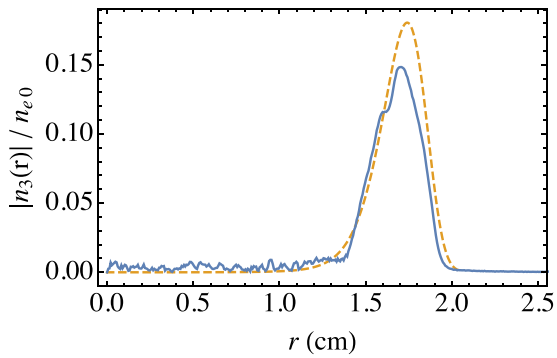

FIG. 18. Solid curve: Fourier component $n_3(r)$ of the vorticity measured from the image in Fig. 17. Dashed curve—diocotron eigenfunction $A_p n_{3,K}(r)$, with $A_p = 0.03$ as determined from Eq. (19) applied to $n(r, \theta)$ for $l = 3$.

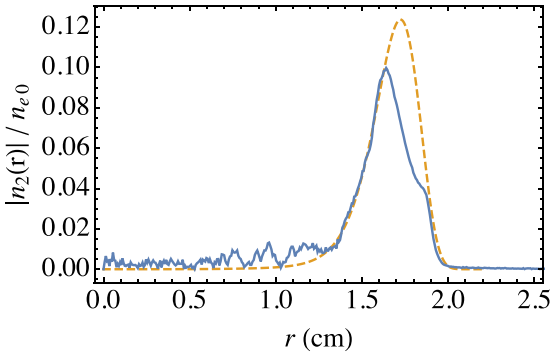

FIG. 19. Solid curve: Fourier component $n_2(r)$ of the vorticity measured from the image in Fig. 17. Dashed curve—diocotron eigenfunction $A_d n_{2,K}(r)$, with $A_d = 0.02$ as determined from Eq. (19) applied to $n(r,\theta)$ for $l=2$.

significantly worse for $e=1$ because of the larger edge density gradient in the model].

For the $l=1$ beat wave, a signal can also be observed in Fig. 20 above the level of noise in the data. The signal has peaks in similar locations to those predicted by the theory (dashed), and in particular, the experimental peak at 1.62 cm is close to the beat wave resonant radius $r_{beat} = 1.7$ cm. The small discrepancy could easily be due to a slightly different radial vorticity profile used in the theory as compared to this particular experimental shot. However, the experimental peak at the beat wave resonance is considerably lower and broader than the theory predicts. We believe that the explanation for this discrepancy may be a nonlinear trapping effect, described below.

The dump diagnostic was triggered at the end of the decay experiment, when perturbations are no longer growing exponentially due to nonlinear saturation. The discrepancy between the theoretical and experimental beat wave peak widths may therefore be related to nonlinear effects not kept in the theory of linear Landau resonance. One such effect is pump depletion, the reduction in pump wave amplitude caused by the growth of the daughter and beat waves, which plays an important role in the saturation of the instability. However, we refer to

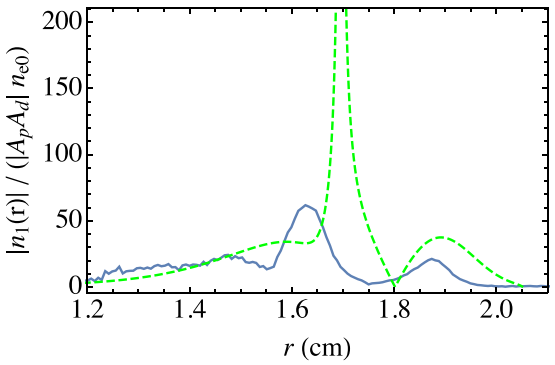

FIG. 20. Solid curve: Absolute value of the beat wave vorticity perturbation $n_1(r)$ measured from the image in Fig. 17, scaled by the amplitudes $A_d = 0.02$ and $A_p = 0.03$ of the diocotron daughter and pump wave. Dashed curve—absolute value of the $l=1$ beat wave component to the unstable vorticity eigenmode (the absolute value of the $A_p = 0.03$ function displayed in Fig. 7).

a different nonlinear effect: nonlinear Landau damping, i.e., cat's eye formation due to trapping of vorticity in the beat wave. To investigate this further, we consider the stream function in the frame of the beat wave, taking $\bar{\theta} = \theta - \Delta\omega t$. The stream function then has the form, to first order in A_p and A_d,

$$\phi(r,\bar{\theta},t) - \phi_e(r) - \frac{1}{2}\Delta\omega r^2 = \phi_1(r)e^{i\bar{\theta}} + A_d\phi_{2,K}(r)e^{2i\bar{\theta}-i(\omega_d-2\Delta\omega)t)} + A_p\phi_{3,K}(r)e^{3i\bar{\theta}-i(\omega_p-3\Delta\omega)t)} + \text{c.c.} \tag{111}$$

For radii near the beat wave resonance, where $-r_{beat}^{-1}\phi_e'(r_{beat}) = \omega_E(r_{beat}) = \Delta\omega$, the $l=0$ stream function can be Taylor expanded, yielding

$$\phi(r,\bar{\theta},t) + \frac{1}{2}r_{beat}\omega_e'(r_{beat})(r-r_{beat})^2 = \phi_1(r)e^{i\bar{\theta}} + A_d\phi_{2,K}(r)e^{2i\bar{\theta}-i(3\omega_d-2\omega_p)t)} + A_p\phi_{3,K}(r)e^{3i\bar{\theta}-i(3\omega_d-2\omega_p)t)} + \text{c.c.} \tag{112}$$

The $l=\pm 2$ and $l=\pm 3$ components to the stream function are nonresonant, so we will ignore them and focus on the resonant beat wave stream function only, which has the form of a pendulum Hamiltonian. Contours of this stream function in the $r-\theta$ plane are displayed in Fig. 21, superimposed on the theoretical beat wave density perturbation $\Re\{\hat{n}_1(r)e^{i\bar{\theta}}/n_{e0}\}$. This can be compared to the experimentally measured density perturbation shown in the same figure. The cat's eye observable in the stream function contours is of similar width to the density features in the experimental data, indicating the possibility that nonlinear Landau damping has saturated the instability. To investigate this further, an estimate of the trapping frequency ω_t in the cat's eye follows from the stream function:

$$\omega_t = \sqrt{-2\omega_e'(r_{beat})|\phi_1(r_{beat})|/r_{beat}} \approx 0.6\sqrt{A_dA_p}\,\omega_{e_0}. \tag{113}$$

For $A_d = 0.02, A_p = 0.03$, the trapping frequency is roughly 6 times the theory growth rate for $3 \to 2$ decay (see Table I), which is consistent with the possibility that cat's eye formation in nonlinear Landau damping is responsible for the broadening of the observed resonant density peak, and plays a role in the saturation of the instability. In this case, the width of the cat's eye, $\omega_t/|\omega_e'(r_{beat})| \approx 0.05$ cm, replaces the linear resonance width $\gamma/|\omega_e'(r_{beat})|$ of the beat wave, roughly consistent with the observed width of the beat wave density features. Nonlinear Landau damping has also been shown to cause the saturation of linear plasma kinetic instabilities such as the bump on tail instability.[43] A more detailed analysis of the effect of nonlinear Landau damping on the growth and saturation of the beat wave instability will be pursued in future work.

V. DISCUSSION

We have presented new experiments and theory investigating the beat wave decay instability of Kelvin/diocotron modes on a two-dimensional vortex, in which a Kelvin/diocotron pump wave decays into a smaller wavenumber Kelvin/diocotron daughter wave and a Landau-damped beat wave at the difference frequency and difference wavenumber between the pump and daughter waves. This is an example of the general process of self-organization in 2D fluid flow, where energy is transferred from small scales to larger scales (the "inverse

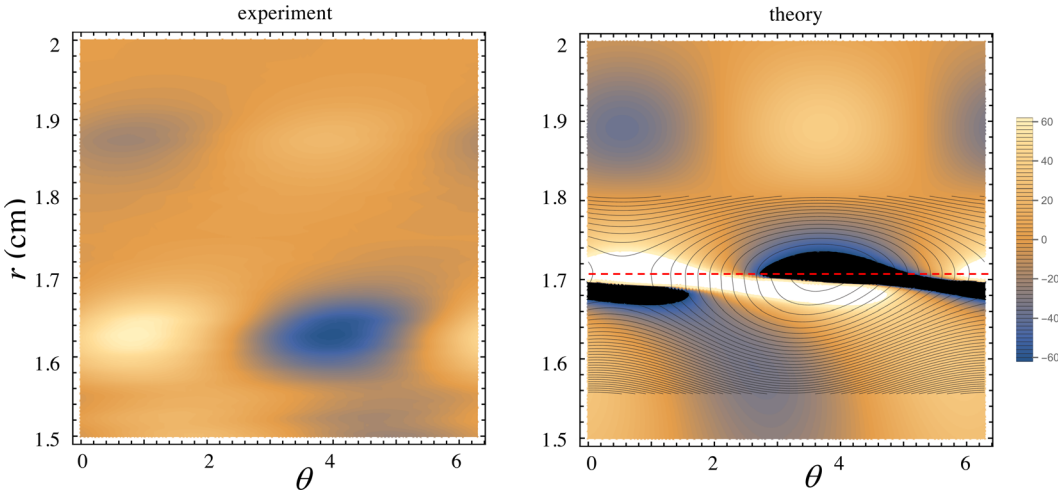

FIG. 21. Color contour maps of the theory (right) and experimental measurement (left) of $\Re\{n_1(r)e^{j\theta}/(n_{e0}A_pA_d)\}$. Contours of the resonant beat wave stream function given by Eq. (112) are superimposed on the theory density, indicating the region of cat's eye formation expected for wave amplitudes $A_d = 0.02$ and $A_p = 0.03$. The dashed line is the theoretical beat wave resonant radius r_{beat}; the experimental resonant radius is smaller by about 0.8 mm.

cascade"[44]) By working in the frame of the pump wave, in which the wave is a stationary equilibrium at early times, the Kelvin/diocotron daughter wave and the beat wave were described as two Fourier components of a single eigenmode of the perturbed pump wave equilibrium. Using this approach, explicit, physically intuitive expressions for the growth rate of the instability and the functional form of the beat wave were derived and compared to nonneutral plasma experiments that measured the growth rate, and that also observed the beat wave. Measured growth rates for a range of beat wave decay processes were in quantitative agreement with theory, within the scatter of the experimental data.

Nonlinear frequency shifts of both the pump and daughter waves were also derived, and through comparison with particle in cell simulations it was found that frequency shifts for pump waves on a vortex patch differ from those for a vortex with a more realistic rounded edge when pump amplitudes become sufficiently large so that vorticity in the edge begins to become trapped in cat's eyes. This effect becomes more important for higher mode number pump waves, where the resonant radius for spatial Landau damping approaches the edge of the vortex.

A discrepancy between the theory and experimental measurements of the beat wave vorticity perturbation was also observed. A possible explanation of this discrepancy is that the measurements were taken in the late stages of the beat wave decay, where nonlinear Landau damping (cat's eye formation) had time to broaden the beat wave vorticity perturbation compared to the theoretical model, which describes only the earlier linear Landau damping stage of the instability. In future work, we intend to study this instability saturation mechanism in more detail, for example, through numerical simulation.

Beat wave decay was shown in this paper to be dependent on a Landau resonance between the beat wave and the plasma rotation rate. It would, therefore, be of interest to consider what the effect would be on the instability of modifying this resonance process. In recent work,[45,46] it has been observed that externally applied time-independent asymmetries in the stream function can produce a slow radial flux of vorticity that strongly modifies the Landau damping of Kelvin/diocotron modes, resulting in algebraic rather than exponential damping. The effect of such a flux on the growth rate of the beat wave instability could be substantial and will be considered in future theory and experiments.

ACKNOWLEDGMENTS

We are grateful for useful conversations with Professor T. M. O'Neil regarding the theory of nonlinear Landau damping and Dr. John Moody regarding previous work on nonlinear decay processes. This work was supported by NSF Grant No. PHY 2106332.

AUTHOR DECLARATIONS

Conflict of Interest

The authors have no conflicts to disclose.

Author Contributions

Daniel H. E. Dubin: Writing – original draft (lead); Writing – review & editing (lead). **Andrey A. Kabantsev:** Investigation (equal); Validation (equal). **Charles Fred Driscoll:** Project administration (equal); Supervision (equal).

DATA AVAILABILITY

The data that support the findings of this study are available from the corresponding author upon reasonable request.

APPENDIX: GREENS FUNCTION SOLUTION FOR THE BEAT WAVE, AND THE FUNCTIONAL FORM OF $\epsilon_l(r)$

Equations (75) and (76) can be formally solved for the scaled beat wave vorticity $\hat{n}_{l_b}(r)$ and stream function $\hat{\phi}_{l_b}(r)$ via a Greens function, providing some analytic insight, as well as the functional form for the function $\epsilon_l(r)$. Breaking $\hat{\phi}_{l_b}$ into real and imaginary parts, $\hat{\phi}_{l_b} = \hat{\phi}_r + i\hat{\phi}_i$, Eqs. (75), (76), and (74) yield

$$\frac{\partial^2\hat{\phi}_r}{\partial r^2}+\frac{1}{r}\frac{\partial\hat{\phi}_r}{\partial r}-\frac{l_b^2}{r^2}\hat{\phi}_r+\frac{s\hat{\phi}_r+F_{b,K}}{\bar{\omega}_{-l_d,K}-l_b\bar{\omega}_e}+\pi\delta(\bar{\omega}_{-l_d,K}-l_b\bar{\omega}_e)s\hat{\phi}_i=0, \tag{A1}$$

$$\frac{\partial^2\hat{\phi}_i}{\partial r^2}+\frac{1}{r}\frac{\partial\hat{\phi}_i}{\partial r}-\frac{l_b^2}{r^2}\hat{\phi}_i+\frac{s\hat{\phi}_i}{\bar{\omega}_{-l_d,K}-l_b\bar{\omega}_e}-\pi\delta(\bar{\omega}_{-l_d,K}-l_b\bar{\omega}_e)(s\hat{\phi}_r+F_{b,K})=0, \tag{A2}$$

where $s(r)=l_bn_e'/r$, and resonances are evaluated using only their principal parts. We can solve these coupled equations using a Greens function $g(r,r')$, which satisfies

$$\frac{\partial^2 g}{\partial r^2}+\frac{1}{r}\frac{\partial g}{\partial r}-\frac{l_b^2}{r^2}g+\frac{P}{\bar{\omega}_{-l_d,K}-l_b\bar{\omega}_e}sg=\delta(r-r'). \tag{A3}$$

In terms of this Greens function the real and imaginary beat wave stream functions are

$$\hat{\phi}_i(r)=g(r,r_{beat})\frac{\pi}{|l_b\omega_e'(r_{beat})|}\times\left[s(r_{beat})\hat{\phi}_r(r_{beat})+F_{b,K}(r_{beat})\right], \tag{A4}$$

$$\hat{\phi}_r(r)=-\mathcal{P}\int_0^{r_w}dr'\frac{g(r,r')F_{b,K}(r')}{\bar{\omega}_{-l_d,K}-l_b\bar{\omega}_e(r')}-\frac{\pi}{|l_b\omega_e'(r_{beat})|}s(r_{beat})\hat{\phi}_i(r_{beat})g(r,r_{beat}). \tag{A5}$$

When Eqs. (A4) and (A5) are evaluated at $r=r_{beat}$ they can be combined to yield a closed-form expression for $\hat{\phi}_r(r_{beat})$:

$$\hat{\phi}_r(r_{beat})=-\frac{\mathcal{P}\int_0^{r_w}dr'\frac{g(r_{beat},r')F_{b,K}(r')}{\bar{\omega}_{-l_d}-l_b\bar{\omega}_e(r')}+\left(\frac{\pi g(r_{beat},r_{beat})}{l_b\omega_e'(r_{beat})}\right)^2 s(r_{beat})F_{b,K}(r_{beat})}{1+\left(\frac{\pi g(r_{beat},r_{beat})s(r_{beat})}{l_b\omega_e'(r_{beat})}\right)^2}. \tag{A6}$$

This expression for $\hat{\phi}_r(r_{beat})$ can then be used in Eq. (A4) to obtain a closed-form expression for the imaginary beat wave stream function $\hat{\phi}_i(r)$,

$$\hat{\phi}_i(r)=g(r,r_{beat})\frac{\pi}{|l_b\omega_e'(r_{beat})|}\times\frac{F_{b,K}(r_{beat})-s(r_{beat})\mathcal{P}\int_0^{r_w}dr'\frac{r'}{r_{beat}}\frac{g(r',r_{beat})F_{b,K}(r')}{\bar{\omega}_{-l_d,K}-l_b\bar{\omega}_e(r')}}{1+\left(\frac{\pi g(r_{beat},r_{beat})s(r_{beat})}{l_b\omega_e'(r_{beat})}\right)^2}, \tag{A7}$$

where we applied the identity $g(r_{beat},r')=g(r',r_{beat})r'/r_{beat}$.

Note that $-bg(r,r_{beat})$ solves the same differential equation as the continuum eigenmode stream function $\phi_{l_b,\alpha}$ for resonant radius $r_{l_b,\alpha}=r_{beat}$; compare Eq. (A3) and Eq. (25). This implies that $\hat{\phi}_i$ is proportional to this continuum eigenmode stream function, i.e.,

$$\hat{\phi}_i(r)=C\phi_{l,\alpha}(r) \tag{A8}$$

for some constant of proportionality C, and thus $\hat{n}_i(r)=Cn_{l,\alpha}(r)$ also. Substituting $g(r,r_{beat})=-\phi_{l_b,\alpha}/b$ into Eq. (A7), and applying the definition s, we can write this constant of proportionality as

$$C=-\frac{\pi C_{\alpha d}}{|l_b\omega_e'(r_\alpha)|}\left.\frac{n_e'(r_\alpha)}{\pi r_\alpha^2\bar{\omega}_e(r_\alpha)b^2\left[1+\left(\frac{\pi c\phi_{l_b,\alpha}(r_\alpha)n_e'(r_\alpha)}{br_\alpha B\omega_e'(r_\alpha)}\right)^2\right]}\right|_{r_\alpha=r_{beat}}. \tag{A9}$$

Here we have related $C_{\alpha d}$ to C by applying Eq. (33) to Eq. (60), yielding

$$\begin{aligned}C_{\alpha d}&=\frac{\bar{\omega}_{l_b,\alpha}}{l_b}\langle n_{l_b,\alpha},F_{b,K}\rangle_P\\&=\frac{\pi\bar{\omega}_{l_b,\alpha}}{l_b}\int r^2dr\frac{n_{l_b,\alpha}F_{b,K}}{n_e'}\\&=\frac{\pi\bar{\omega}_e(r_\alpha)r_\alpha^2b}{n_e'(r_\alpha)}\left[F_{b,K}(r_\alpha)+\frac{s(r_\alpha)}{br_\alpha}\int Pr'dr'\frac{\phi_{l_b,\alpha}(r')F_{b,K}(r')}{\bar{\omega}_{-l_d,K}-l_b\bar{\omega}_e(r')}\right]\end{aligned} \tag{A10}$$

and where in the second line we substituted for $n_{l_b,\alpha}$ using Eq. (24), used the definition s, and applied the resonance conditions $r_\alpha=r_{beat}$, and $l_b\bar{\omega}_e(r_\alpha)=\bar{\omega}_{l_b,\alpha}=\bar{\omega}_{-l_d,K}$. The quantity in the square bracket appears in the numerator of Eq. (A7), leading to Eq. (A9).

Equation (A9) allows us to connect the new expression for the growth rate, the imaginary part of Eq. (77), to the old expression Eq. (69). The imaginary part of the radial integral in Eq. (79) is determined by $\hat{n}_i$ and $\hat{\phi}_i$, which are proportional to the resonant continuum eigenmode vorticity and stream function, respectively, $(\hat{n}_i,\hat{\phi}_i)=C(n_{l_b,\alpha},\phi_{l_b,\alpha})$, see Eq. (A8). This implies that the imaginary part of the inner product appearing in Eq. (77) is $\Im\langle n_{b,K},\hat{F}_d\rangle_{\bar{E}}=C\langle n_{b,K},F_{d,\alpha}\rangle_{\bar{E}}=CC_{d\alpha}$, where in the last step we used the definition of $C_{d\alpha}$, Eq. (62). Thus, the imaginary part of Eq. (77) yields

$$\gamma=A_p^2\frac{CC_{d\alpha}}{\bar{E}_{l_d,K}}. \tag{A11}$$

Comparing this expression to Eq. (69) after applying Eq. (A9), we see that the two expressions for the growth rate are identical *provided that* Eq. (40) for $\epsilon_l(r_\alpha)$ is satisfied, for $l=l_b$. This argument

provides a (somewhat roundabout) method for determining the proper functional form of $\epsilon_l(r_\alpha)$.

REFERENCES

[1]P. B. Rhines, "Vorticity dynamics of the oceanic general circulation," Annu. Rev. Fluid Mech. **18**, 433 (1986); A. Fujisawa, "A review of zonal flow experiments," Nucl. Fusion **49**, 013001 (2009).

[2]J. C. McWilliams, "The emergence of isolated coherent vortices in turbulent flow," J. Fluid Mech. **146**, 21(1984); K. S. Fine, C. F. Driscoll, J. H. Malmberg, and T. B. Mitchell, "Measurements of symmetric vortex merger," Phys. Rev. Lett. **67**, 588 (1991).

[3]K. S. Fine, A. C. Cass, W. G. Flynn, and C. F. Driscoll, "Relaxation of 2D turbulence to vortex crystals," Phys. Rev. Lett. **75**, 3277 (1995); L. Siegelman, W. R. Young, and A. P. Ingersoll, "Polar vortex crystals: Emergence and structure," Proc. Natl. Acad. Sci. U. S. A. **119**, e2120486119 (2022).

[4]C. E. Leith, "Minimum enstrophy vortices," Phys. Fluids **27**, 1388 (1984); S. J. Zweben, "Search for coherent structure within tokamak plasma turbulence," Phys. Fluids **28**, 975 (1984); P. S. Marcus, T. Kundu, and C. Lee, "Vortex Dynamics and Zonal Flow," Phys. Plasmas **7**, 1630 (2000); B. Eliason and P. K. Shukla, "Formation and dynamics of coherent structures involving phase-space vortices in plasmas," Phys. Rep. **422**, 225 (2006).

[5]M. V. Melander, J. C. McWilliams, and N. J. Zabusky, "Axisymmetrization and vorticity-gradient intensification of an isolated two-dimensional vortex through filamentation," J. Fluid Mech. **178**, 137 (1987).

[6]H. B. Yao and N. J. Zabusky, "Axisymmetrization of an isolated vortex region by splitting and partial merging of satellite depletion perturbations," Phys. Fluids **8**, 1842 (1996).

[7]R. R. Trieling, G. J. F. van Heijist, and Z. Kizner, "Laboratory experiments on multipolar vortices in a rotating fluid," Phys. Fluids **22**, 094104 (2010).

[8]J. Bedrossian, M. Coti Zelati, and V. Vicol, "Vortex axisymmetrization, inviscid damping, and vorticity depletion in the linearized 2D Euler equations," Ann. PDE **5**, 4 (2019).

[9]D. A. Schecter and M. T. Montgomery, "On the symmetrization rate of an intense geophysical vortex," Dyn. Atmos. Oceans **37**, 55 (2003).

[10]X.-P. Huang, K. S. Fine, and C. F. Driscoll, "Coherent vorticity holes from 2D turbulence decaying in a background shear flow," Phys. Rev. Lett. **74**, 4424 (1995).

[11]D. A. Schecter, D. H. E. Dubin, A. C. Cass, C. F. Driscoll, I. M. Lansky, and T. M. O'Neil, "Inviscid damping of asymmetries on a two-dimensional vortex," Phys. Fluids **12**, 2397 (2000).

[12]R. J. Briggs, J. D. Daugherty, and R. H. Levy, "Role of Landau damping in crossed-field electron beams and inviscid shear flow," Phys. Fluids **13**, 421 (1970).

[13]N. Mattor, B. T. Chang, and T. B. Mitchell, "Beat-wave resonant down scattering of diocotron and Kelvin modes," Phys. Rev. Lett. **96**, 045003 (2006).

[14]T. B. Mitchell and C. F. Driscoll, "Symmetrization of 2D vortices by beat-wave damping," Phys. Rev. Lett. **73**, 2196 (1994).

[15]G. Maero, N. Panzeri, L. Patricelli, and M. Rome, "Resonant excitation of single Kelvin–Helmholtz high-order waves in a magnetized electron fluid vortex," J. Plasma Phys. **89**, 935890601 (2023).

[16]R. Levy, "Diocotron instability in a cylindrical geometry," Phys. Fluids **8**, 1288 (1965); "Two new results in cylindrical diocotron theory," **11**, 920 (1968).

[17]R. Z. Sagdeev and A. A. Galeev, *Nonlinear Plasma Theory* (W. A. Benjamin, New York, 1969), p. 5.

[18]M. Case, "Stability of inviscid plane Couette flow," Phys. Fluids **3**, 143 (1960).

[19]B. Coppi, M. N. Rosenbluth, and R. N. Sudan, "Nonlinear interactions of positive and negative energy modes in rarefied plasmas (I)," Ann. Phys. **55**, 207 (1969).

[20]R. C. Davidson, *Methods in Nonlinear Plasma Theory* (Academic Press, New York, 1972), Chap. 13.

[21]T. S. Hahm and W. M. Tang, "Weak turbulence theory of collisionless trapped electron driven drift instability in tokamaks," Phys. Fluids B **3**, 989 (1991).

[22]R. P. H. Chang and M. Porkolab, "Experimental observation of nonlinear landau damping of plasma waves in a magnetic field," Phys. Rev. Lett. **25**, 1262 (1970).

[23]N. Mattor and T. B. Mitchell, "Scattering of spiral density waves to lower arm number," Astrophys. J. **472**, 532 (1996).

[24]A. E. H. Love, "On the stability of certain vortex motions," Proc. London Math. Soc. **s1-25**, 18 (1893).

[25]G. B. Whitham, *Linear and Nonlinear Waves* (Wiley Interscience, New York, 1999).

[26]D. H. E. Dubin, "Parametric instability driven by weakly trapped particles in nonlinear plasma waves," Phys. Rev. Lett. **121**, 015001 (2018).

[27]D. H. E. Dubin, "Instability of nonlinear Trivelpiece-Gould waves I: Wave degeneracies," Phys. Plasmas **26**, 102111 (2019).

[28]R. C. Davidson, *Theory of Nonneutral Plasmas* (Benjamin, Reading, 1974), Sec. 2.10.

[29]N. G. van Kampen, "On the theory of stationary waves in plasmas," Physics **21**, 949 (1955).

[30]D. H. E. Dubin, "Normal modes, rotational inertia, and thermal fluctuations of trapped ion crystals," Phys. Plasmas **27**, 102107 (2020).

[31]D. H. E. Dubin, "Nonlinear processes in Trivelpiece-Gould waves," Phys. Plasmas (unpublished).

[32]H. Lamb, *Hydrodynamics*, 6th ed. (Dover, New York, 1932), p. 232.

[33]J. Burbea, "Motions of vortex patches," Lett. Math. Phys. **6**, 1 (1982).

[34]K. S. Fine, "Simple theory of a nonlinear diocotron mode," Phys. Fluids B **4**, 3981 (1992).

[35]D. Z. Jin and D. H. E. Dubin, "Point vortex dynamics within a background vorticity patch," Phys. Fluids **13**, 677 (2001).

[36]G. S. Deem and N. J. Zabusky, "Vortex waves: Stationary " V states," interactions, recurrence, and breaking," Phys. Rev. Lett. **40**, 859 (1978).

[37]T. B. Mitchell, Ph.D. thesis (Department of Physics, University of California San Diego, 1993).

[38]T. B. Mitchell and L. F. Rossi, "The evolution of Kirchhoff elliptic vortices," Phys. Fluids **20**, 054103 (2008).

[39]J. Burbea and M. Landau, "The Kelvin waves in vortex dynamics and their stability," J. Comput. Phys. **45**, 127 (1982).

[40]I. B. Bernstein, J. M. Green, and M. D. Kruskal, "Exact nonlinear plasma oscillations," Phys. Rev. **108**, 546 (1957).

[41]D. H. E. Dubin, *Numerical and Analytical Methods for Scientists and Engineers* (Wiley, New York, 2003), Chap. 5, problem 18.

[42]W. D. White, J. D. Malmberg, and C. F. Driscoll, "Resistive-wall destabilization of diocotron waves," Phys. Rev. Lett. **49**, 1822 (1982).

[43]T. M. O'Neil, J. H. Winfrey, and J. H. Malmberg, "Nonlinear interaction of a small cold beam and a plasma," Phys. Fluids **14**, 1204 (1971).

[44]R. H. Kraichnan and D. Montgomery, "Two-dimensional turbulence," Rep. Prog. Phys. **43**, 547 (1980).

[45]A. A. Kabantsev, C. Y. Chim, T. M. O'Neil, and C. F. Driscoll, "Diocotron and Kelvin mode damping from a flux through the critical layer," Phys. Rev. Lett. **112**, 115003 (2014).

[46]C. Y. Chim and T. M. O'Neil, "Flux-driven algebraic damping of m = 2 diocotron mode," Phys. Plasmas **28**, 092105 (2021).